The Astrophysical Journal, 669:959–981, 2007 November 10

WARM MOLECULAR HYDROGEN IN THE *SPITZER* SINGS GALAXY SAMPLE

H. Roussel,[1] G. Helou,[2] D. J. Hollenbach,[3] B. T. Draine,[4] J. D. Smith,[5] L. Armus,[2] E. Schinnerer,[1] F. Walter,[1] C. W. Engelbracht,[5] M. D. Thornley,[6] R. C. Kennicutt,[5,7] D. Calzetti,[8] D. A. Dale,[9] E. J. Murphy,[10] and C. Bot[2]

Received 2007 February 18; accepted 2007 July 3

ABSTRACT

Results on the properties of warm molecular hydrogen in 57 normal galaxies are derived from measurements of H_2 rotational transitions, obtained as part of SINGS. This study extends previous extragalactic surveys of emission lines of H_2 to fainter and more common systems ($L_{FIR} = 10^7$–6×10^{10} $L_\odot$). The 17 μm $S(1)$ transition is securely detected in the nuclear regions of 86% of galaxies with stellar masses above $10^{9.5}$ $M_\odot$. The derived column densities of warm H_2 ($T \geq 100$ K), although averaged over kiloparsec-scale areas, are commensurate with values observed in resolved photodissociation regions. They amount to between 1% and >30% of the total H_2. The power emitted in the three lowest energy transitions is on average 30% of the power of the bright [Si II] cooling line (34.8 μm) and about 4×10^{-4} of the total infrared power for star-forming galaxies, which is consistent with excitation in PDRs. The fact that the H_2 line intensities scale tightly with the aromatic band emission, even though the average radiation field intensity varies by a factor of 10, can also be understood if both tracers originate predominantly in PDRs, either dense or diffuse. Many of the 25 LINER/Seyfert targets strongly depart from the rest of the sample, in having warmer excited H_2 and excess H_2 rotational power with respect to the dust emission. We propose a threshold in H_2–to–aromatic band power ratios, allowing the identification of low-luminosity AGNs by an excess H_2 excitation. A dominant contribution from shock heating is favored in these objects. Finally, we detect in nearly half the star-forming targets nonequilibrium ortho-to-para ratios, consistent with the effects of FUV pumping combined with incomplete ortho-para thermalization, or possibly nonequilibrium photodissociation fronts.

Subject headings: galaxies: ISM — infrared: galaxies — infrared: ISM — ISM: lines and bands — ISM: molecules — surveys

Online material: extended figure, machine-readable tables

1. INTRODUCTION

Rotational transitions of molecular hydrogen, lying in the mid-infrared range between 5 and 30 μm (Table 1), provide measurements of the mass and temperature distribution of the bulk of the warm molecular gas phase, at temperatures of ~100–1000 K. By contrast, the transitions from higher vibrational levels in the near-infrared, better studied because more easily observable from the ground, arise from gas at apparent excitation temperatures of more than 1000 K located in a thin layer of molecular clouds, hosting a negligible fraction (of the order of 10^{-6}) of the total H_2 mass (Black & Dalgarno 1976; Burton et al. 1992). The rotational lines are thus more appropriate tracers of molecular gas being exposed to moderate heating, and they arise from a much larger volume fraction of the molecular clouds. They constitute one of the most important coolants of warm molecular gas (Neufeld & Kaufman 1993).

H_2 emission lines have been detected in a wide array of sources, including outflows from young stars (Gautier et al. 1976; Bally & Lane 1982), photodissociation regions (PDRs; Gatley et al. 1987; Tanaka et al. 1989), planetary nebulae (Treffers et al. 1976; Beckwith et al. 1978), supernova remnants (Treffers 1979; Burton et al. 1989), large regions at the centers of galaxies (Thompson et al. 1978; Gatley et al. 1984), and extranuclear large-scale shocks in galaxy collisions (Herbst et al. 1990; Sugai et al. 1997; Appleton et al. 2006). The possible excitation mechanisms are accordingly varied. In normal galaxies, the major excitation source is expected to be the far-ultraviolet (FUV) radiation of massive stars in PDRs, with photon energies between 6 and 13.6 eV (Hollenbach & Tielens 1997 and references therein). H_2 molecules can be pumped by FUV photons into electronically excited states, followed by fluorescence and radiative cascade through the vibration-rotation levels of the ground electronic state. Pure fluorescent spectra are produced only if the cascade is not significantly altered by collisions with hydrogen atoms and molecules; if the critical densities for collisional de-excitation are exceeded, a portion of the pump energy is converted to heat by collisions, and the lowest rotational levels are populated by collisions and thermalized. Pure fluorescence is thus much more likely in the vibrational transitions, which have high critical densities, than in the pure rotational transitions considered here, with critical densities below a few times 10^3 cm^{-3} for $S(0)$ to $S(3)$. In addition, FUV photons can be absorbed by dust grains, followed by the ejection of photoelectrons that heat the gas. This also results in the thermal excitation of the low-energy levels of H_2 by collisions with the warm gas. Besides the radiation of massive stars, a second important source of excitation is shocks, in molecular outflows, supernova remnants, or cloud collisions in a disturbed gravitational potential (Shull & Hollenbach 1978; Draine et al. 1983). In addition to the above processes, X-rays produced in active nuclei or in supernova remnant shocks can partially ionize and heat the gas over large column densities, leading to H_2 excitation by collisions with hydrogen atoms and molecules

[1] Max-Planck-Institut für Astronomie, Heidelberg 69117 Germany; roussel@mpia-hd.mpg.de.
[2] California Institute of Technology, Pasadena, CA 91125.
[3] NASA Ames Research Center, Moffett Field, CA 94035.
[4] Princeton University, Princeton, NJ 08544.
[5] Steward Observatory, University of Arizona, Tucson, AZ 85721.
[6] Bucknell University, Lewisburg, PA 17837.
[7] Institute of Astronomy, University of Cambridge, Cambridge CB3 0HA, UK.
[8] University of Massachusetts, Amherst, MA 01003.
[9] University of Wyoming, Laramie, WY 82071.
[10] Yale University, New Haven, CT 06520.

TABLE 1
OBSERVED H_2 LINES

Transition $v = 0$	Short Notation	Rest λ (μm)	Spectral Order	E_u/k (K)	A (10^{-11} s^{-1})
$J = 2-0$	$S(0)$	28.219	LH 14	510	2.95
$J = 3-1$	$S(1)$	17.035	SH 12	1015	47.6
$J = 4-2$	$S(2)$	12.279	SH 17	1681	275.0
$J = 5-3$	$S(3)$	9.665	SL 1	2503	980.0
$J = 6-4$	$S(4)$	8.025	SL 1	3473	2640.0
$J = 7-5$	$S(5)$	6.910	SL 2	4585	5880.0
$J = 8-6$	$S(6)$	6.109	SL 2	5828	11400.0
$J = 9-7$	$S(7)$	5.511	SL 2	7196	20000.0

NOTE.—The rotational upper level energies were computed from the molecular constants given by Huber & Herzberg (1979), and the transition probabilities are from Black & Dalgarno (1976).

and with fast electrons (Lepp & McCray 1983; Draine & Woods 1991; Maloney et al. 1996). Finally, H_2 molecules can be formed directly into excited states.

Surveys of molecular hydrogen line emission in galaxies have been so far mostly restricted to starbursts, active galactic nuclei (AGNs), and ultraluminous systems and have been performed mostly in the near-infrared, targeting vibration-rotation lines that arise from upper levels with much higher excitation energies than the mid-infrared lines. It has been speculated that the major source of H_2 heating in star-forming galactic nuclei was shocks in supernova remnants, based on comparison of the luminosity of some vibration-rotation H_2 lines with a limited number of Galactic templates and with shock models (Moorwood & Oliva 1988; Mouri et al. 1990). However, scaling individual templates to the integrated emission of galaxies has large inherent uncertainties, and the near-infrared line ratios most often used to discriminate between thermal and nonthermal emission are not always sufficient to distinguish between shocks and fluorescent excitation followed by collisional de-excitation in high-density regions (Sternberg & Dalgarno 1989). Puxley et al. (1988) surveyed starburst galaxies in several vibration-rotation lines and found that the dominant excitation mechanism was pumping by the FUV radiation of massive stars, rather than collisional excitation. Davies et al. (2003) reached the same conclusion for a small sample of ultraluminous galaxies, in which the first vibrational level is thermalized by high densities in PDRs. Active nuclei (LINERs or Seyferts) can show an excess of H_2 emission relative to hydrogen recombination lines and aromatic bands (e.g., Moorwood & Oliva 1988; Larkin et al. 1998), but the exact nature of the additional source of excitation, namely, X-ray excitation, fluorescence induced by a nonthermal ultraviolet continuum, or shocks induced by dynamical perturbations, is often unclear (e.g., Quillen et al. 1999). It is, however, unlikely that significant H_2 emission could arise from interaction between molecular clouds and jets from Seyfert nuclei (Rotaciuc et al. 1991; Knop et al. 2001).

The detection of a rotational line of H_2 was first reported by Beck et al. (1979) [the $S(2)$ transition at 12.3 μm in Orion] from observations at Las Campanas Observatory. It was soon followed by many more ground-based detections, but the majority of data on the rotational spectrum of H_2 were produced by the SWS instrument on board the *Infrared Space Observatory* (*ISO*; e.g., Lutz et al. 2000; Rigopoulou et al. 2002). Furthermore, with previous infrared spectroscopic capabilities, observations of normal galaxies have proven difficult due to sensitivity limitations, so that our current knowledge is mainly extrapolated from studies of very bright objects, maybe not representative of the general galaxy population. The purpose of this paper is thus to extend previous work to fainter systems than formerly accessible and to characterize directly the generic properties of the warm molecular hydrogen content of normal galaxies. The SINGS sample (*Spitzer* Infrared Nearby Galaxies Survey; Kennicutt et al. 2003), covering a broad range of infrared luminosities, morphologies, and nuclear types, is ideally suited to such a pursuit.

Studies of rotational lines alone, without information on vibrational levels, have very limited diagnostic value concerning the source of excitation because the low critical densities of the rotational levels make it likely that they will be thermalized most of the time and thus cannot be used to distinguish between the various heating mechanisms. Because observations of vibration-rotation transitions in the near-infrared are still scarce for normal galaxies, and because they are typically performed in apertures that are not matched to our observations, we did not attempt to include vibrational levels in our analysis. The characterization of excitation mechanisms and physical conditions in the gas would greatly benefit from such information but would necessitate an additional dedicated survey.

The rotational lines are, however, energetically important and can characterize the temperature and density conditions of a large mass fraction of the interstellar medium in galaxies, i.e., that consisting of warm molecular gas. From an SWS survey of rotational lines in nearby starburst and Seyfert galaxies, Valentijn et al. (1996) and Rigopoulou et al. (2002) obtained mass fractions of H_2 in the warm phase of several percent. In ultraluminous galaxies observed with *Spitzer*, Higdon et al. (2006) derive much lower mass fractions of warm gas, but the fact that the majority of their sample has only upper limits for the $S(0)$ line makes it possible that the temperatures are overestimated [because computed from the $S(1)$ to $S(3)$ lines only, whenever $S(0)$ is undetected] and thus the masses of warm H_2 underestimated.

This paper presents observations of warm molecular hydrogen in nearby galaxies obtained as part of SINGS (Kennicutt et al. 2003). From these data, we present quantifications of the temperatures and column densities of warm H_2 encountered in kiloparsec-scale areas, mostly nuclear regions, and a comparison of the power emitted in the rotational lines with those produced by [Si II] at 34.8 μm, which is the dominant cooling line of normal galaxies in the mid-infrared range, and by dust. We emphasize the different properties of star-forming regions and nuclei classified as LINERs or Seyferts and discuss their H_2 excitation mechanisms. The data, analysis methods, and observational results are described in §§ 2–5.[11] The interpretation of the main findings is presented

[11] For easier comparison to future observations and models, ASCII flux tables of all the measured quantities are available on e-mail request.

TABLE 2
TARGETS

Galaxy	D (Mpc)	Class	R.A. (J2000.0)	Decl. (J2000.0)	Solid Angle (arcsec^2)
N24	8.2	Dwarf	00 09 56.31	−24 57 52.0	294.0
N337	24.7	Nuc	00 59 49.99	−07 34 42.5	289.0
N628	11.4	Nuc	01 36 41.72	+15 46 59.4	300.0
N855	9.6	Dwarf	02 14 03.64	+27 52 40.6	288.0
N925	10.1	Nuc	02 27 17.06	+33 34 43.8	287.0
N1097	16.9	Nuc	02 46 18.77	−30 16 30.0	809.0
N1266	31.3	LINER	03 16 00.68	−02 25 38.8	287.0
N1291	9.7	LINER	03 17 18.50	−41 06 27.7	287.0
N1316	26.3	LINER	03 22 41.61	−37 12 28.7	287.0
N1482	22.0	Nuc	03 54 38.68	−20 30 08.5	798.0
N1512	10.4	Nuc	04 03 53.96	−43 20 55.6	831.0
N1566	18.0	Sy	04 20 00.53	−54 56 17.4	306.0
N1705	5.8	Dwarf	04 54 13.26	−53 21 39.2	802.0
N2403	3.5	Nuc	07 36 50.25	+65 36 04.6	287.0
N2798	24.7	Nuc	09 17 22.99	+42 00 00.8	293.0
N2841	9.8	LINER	09 22 02.75	+50 58 35.5	291.0
N2915	2.7	Dwarf	09 26 11.59	−76 37 34.2	291.0
N2976	3.5	Dwarf	09 47 15.63	+67 55 00.3	289.0
N3031	3.5	Sy	09 55 33.50	+69 03 55.8	296.0
N3049	19.6	Nuc	09 54 49.66	+09 16 19.2	320.0
N3184	8.6	Nuc	10 18 17.03	+41 25 28.3	287.0
N3190	17.4	LINER	10 18 05.71	+21 49 56.8	304.0
N3198	9.8	Nuc	10 19 55.10	+45 32 59.6	287.0
N3265	20.0	Nuc	10 31 06.85	+28 47 49.1	301.0
Mrk 33	21.7	Dwarf	10 32 32.02	+54 24 05.4	315.0
N3351	9.3	Nuc	10 43 57.83	+11 42 10.9	761.0
N3521	9.0	LINER	11 05 48.51	−00 02 10.1	285.0
N3621	6.2	LINER	11 18 16.62	−32 48 49.9	291.0
N3627	8.9	Sy	11 20 15.04	+12 59 31.0	301.0
N3773	12.9	Dwarf	11 38 12.91	+12 06 43.0	285.0
N3938	12.2	Nuc	11 52 49.45	+44 07 15.0	292.0
N4125	21.4	LINER	12 08 05.73	+65 10 27.9	294.0
N4254	20.0	Nuc	12 18 49.71	+14 25 01.4	299.0
N4321	20.0	Nuc	12 22 55.08	+15 49 18.2	795.0
N4450	20.0	LINER	12 28 29.51	+17 05 04.9	285.0
N4536	25.0	Nuc	12 34 27.22	+02 11 14.3	777.0
N4552	20.0	LINER	12 35 39.71	+12 33 21.9	285.0
N4559	11.6	Nuc	12 35 57.79	+27 57 36.7	295.0
N4569	20.0	LINER	12 36 49.91	+13 09 46.8	287.0
N4579	20.0	Sy	12 37 43.70	+11 49 07.1	295.0
N4594	13.7	LINER	12 39 59.58	−11 37 22.3	289.0
N4625	9.5	Dwarf	12 41 52.65	+41 16 26.5	294.0
N4631	9.0	Nuc	12 42 07.84	+32 32 34.8	282.0
N4725	17.1	Sy	12 50 26.71	+25 30 03.2	294.0
N4736	5.3	LINER	12 50 53.23	+41 07 13.6	298.0
N4826	5.6	LINER	12 56 43.79	+21 41 00.7	292.0
N5033	13.3	Sy	13 13 27.67	+36 35 38.2	311.0
N5055	8.2	LINER	13 15 49.50	+42 01 46.6	313.0
N5194	8.2	Sy	13 29 52.94	+47 11 44.2	330.0
N5194_A[a]	8.2	H II	13 29 49.54	+47 13 28.6	256.0
N5194_B[a]	8.2	H II	13 30 01.69	+47 12 50.9	271.0
N5194_C[a]	8.2	H II	13 30 00.02	+47 11 11.9	352.0
N5194_D[a]	8.2	H II	13 30 02.76	+47 09 53.0	338.0
N5194_E[a]	8.2	H II	13 29 56.84	+47 10 45.9	234.0
N5194_F[a]	8.2	H II	13 29 52.93	+47 12 38.7	297.0
N5194_G[a]	8.2	H II	13 29 43.99	+47 10 20.7	285.0
N5195	8.2	LINER	13 29 59.80	+47 16 00.1	323.0
N5713	26.6	Nuc	14 40 11.57	−00 17 19.1	292.0
N5866	12.5	LINER	15 06 29.58	+55 45 46.7	286.0
N6822_A[b]	0.6	Dwarf	19 44 52.84	−14 43 09.8	308.0
N6822_B[b]	0.6	Dwarf	19 44 50.57	−14 52 49.0	288.0
N6822_C[b]	0.6	Dwarf	19 44 48.67	−14 52 26.5	304.0
N6946	5.5	Nuc	20 34 51.79	+60 09 12.6	803.0
N7331	15.7	LINER	22 37 04.11	+34 24 57.5	263.0
N7552	22.3	Nuc	23 16 10.56	−42 35 04.0	722.0
N7793	3.2	Dwarf	23 57 49.79	−32 35 28.4	296.0

NOTES.—Units of right ascension are hours, minutes, and seconds, and units of declination are degrees, arcminutes, and arcseconds. Distances are from Kennicutt et al. (2003). Nuclear classifications derived from optical spectroscopy, published by Smith et al. (2007a), were modified for the following targets. N1097, N1512, N4321, and N7552: since our aperture includes a bright star-forming ring, which dominates the dust and line emission, we adopt the H II class instead of the LINER class. N2841, N4552, N4569, N4594, N4826, and N5195: the Sy class was changed to LINER (Ho et al. 1997). N3198 and N3938: the LINER class was changed to H II (Ho et al. 1997). The dwarf galaxy class is here arbitrarily defined by a total stellar mass, estimated by Lee et al. (2006) as below $10^{9.7}\ M_{\odot}$.

[a] A total of 11 extranuclear regions were observed in high-resolution spectroscopy in NGC 5194, from which we included seven in our sample.

[b] Several locations were observed in high-resolution spectroscopy in this galaxy. We present here results for three among the brightest regions at 7.9 and 24 μm. N6822_A corresponds to the H II region Hubble V (Hubble 1925), and N6822_C to the H II region Kγ (Kinman et al. 1979).

in §§ 6 and 7, and a summary of the results and conclusions can be found in § 8.

2. DATA AND MEASUREMENTS

2.1. *Targets*

The SINGS sample (Kennicutt et al. 2003), comprising 75 galaxies, is intended to be a valuable representative set of local galaxies that are not ultraluminous, and whose moderate distances ensure that the properties of the interstellar medium can be studied at relatively small spatial scales (a few hundreds of parsecs at the shortest wavelengths). Numerous sources with mild starbursts or low-luminosity active nuclei are included. Of this sample, we excluded from the present study the objects that were not observed in spectroscopic mode because of their very low brightness (DDO 154, Ho I, M81 dwA, M81 dwB), or containing very little dust and nebular emission within the nuclear area mapped by the high spectral resolution modules (the quiescent ellipticals NGC 584 and NGC 1404, the quiescent dwarf galaxies DDO 53, DDO 165, and Ho IX, and the asymmetric Magellanic galaxies NGC 4236, NGC 5398, NGC 5408, and IC 4710). The dwarf galaxies IC 2574 and NGC 5474 were also rejected because they lack observations in some of the spectroscopic modules. Of the two star-forming dwarf galaxies with several extranuclear pointings, Ho II and NGC 6822, we retained only NGC 6822 here; the regions within Ho II are indeed two faint to allow an analysis of the H_2 excitation diagram, contrary to some regions within NGC 6822. Low-mass galaxies with extranuclear pointings will be discussed elsewhere. NGC 3034 (M82) was excluded due to the unavailability of nuclear spectroscopy from SINGS, as well as NGC 1377, which constitutes a galaxy class of its own very different from the rest of the SINGS sample, and which has been discussed separately (Roussel et al. 2006). The sample for H_2 measurements comprises 66 targets in 57 galaxies (Table 2). The pointings are centered either on the nuclear regions (for most targets) or on some bright star-forming complexes (for a few dwarf galaxies and a

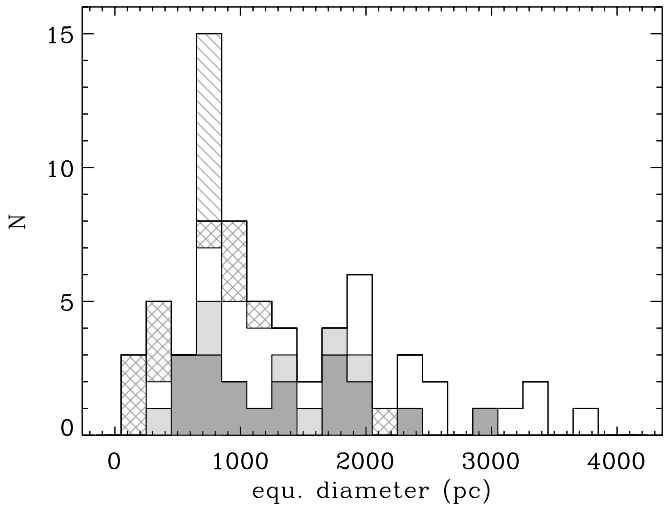

FIG. 1.—Histogram of the equivalent diameters of the areas over which the line and continuum fluxes were integrated. The apertures were defined by the intersection of the spectral maps in the LH, SH, and SL modules of the IRS instrument. The extranuclear regions in NGC 5194 are shown by the hatched histogram, the regions within dwarfs by the cross-hatched histogram, the LINER nuclei by the darker shade, and the Seyfert nuclei by the lighter shade.

spiral galaxy). Diffuse regions within galactic disks are not covered by the present study.

The aperture over which we extracted the spectra is the intersection of the various areas covered by all four spectroscopic modules. The central position and solid angle of this aperture, used to measure all the quantities presented in this paper (line and continuum fluxes), are listed for each galaxy in Table 2. In practice, the limiting size is that of the maps performed with the high-resolution modules, which were enlarged in a few cases in order to cover the emission from a star-forming circumnuclear ring. At the distances of the targets, the equivalent linear diameters of the apertures range from 60 pc to 3.8 kpc (distribution shown in Fig. 1), and the median is 900 pc. Although the apertures are in general small fractions of the optical extent of the galaxies, the measurements are still averages over very large and complex areas. It is expected that a large number of disconnected star formation sites, in addition to the nucleus, contribute to the total emission.

2.2. *Broadband Imaging*

To estimate flux densities of the dust continuum and of the aromatic bands (also referred to as the emission from PAHs, or polycyclic aromatic hydrocarbons), we used images in the 3.6 and 7.9 μm bands of the IRAC camera (Fazio et al. 2004) and scan maps in the three bands of the MIPS instrument (Rieke et al. 2004) at effective wavelengths of 24, 71, and 156 μm. Since in early-type galaxies photospheric emission can make an important contribution to 7.9 μm fluxes, we subtracted an estimate of this component in order to obtain pure measurements of aromatic band emission. To this effect, we scaled 3.6 μm fluxes, assumed to be dominated by stellar emission, as described in Helou et al. (2004). The resulting flux densities are noted $F_{7.9,\mathrm{dust}}$.

The observing strategy and data reduction are described by Kennicutt et al. (2003). The full width at half-maximum of the point-spread function (PSF) is close to $2''$ at 7.9 μm, $6''$ at 24 μm, $18''$ at 71 μm, and $40''$ at 156 μm. Flux calibration uncertainties are of the order of 10% in the IRAC bands and 5%, 10%, and 15% in the MIPS 24, 71, and 156 μm bands, respectively. To correct for the effects of light scattering in IRAC arrays, we applied to flux densities measured from IRAC maps corrective factors that are appropriate for the photometry of extended sources within apertures of arbitrary size (derived by T. Jarrett and published by Dale et al. 2007). For our apertures, the correction factor at 7.9 μm is of the order of 10%.

2.3. *Spectroscopic Data*

The targets were observed in mapping mode with the IRS instrument (Houck et al. 2004), at low spectral resolution between 5 and 38 μm, with the SL and LL slits ($\lambda/\Delta\lambda \approx 60$–$130$), and at high spectral resolution between 10 and 37 μm, with the SH and LH slits ($\lambda/\Delta\lambda \approx 600$). The observing strategy is described by Kennicutt et al. (2003) and Smith et al. (2004). The data were preprocessed with the S13 version of the *Spitzer* Science Center pipeline. Pixels with an abnormal responsivity were masked, and spectral cubes were built with the Cubism software (Smith et al. 2007b). The flux calibration was performed as described by Roussel et al. (2006). We checked the accuracy of this procedure by systematically comparing broadband fluxes from imaging observations and from spectra, and line fluxes from high and low spectral resolution spectra, for bright lines that are minimally contaminated by broad aromatic features at low resolution (but note that even if the flux calibrations of the different modules were in perfect agreement, deviations would be expected from slight misalignment between the apertures). We obtain $F_{24}(\mathrm{MIPS})/F_{24}(\mathrm{LL}) = 1.01 \pm 0.04$ (for targets with $F_{24} > 0.025$ Jy within a diameter of about $50''$), $F_{7.9}(\mathrm{IRAC})/F_{7.9}(\mathrm{SL}) = 0.99 \pm 0.05$ (for targets with $F_{7.9} > 0.025$ Jy within a diameter of about $30''$ and accurately determined backgrounds in SL maps), $F_{[\mathrm{Si\ II}]}(\mathrm{LL})/F_{[\mathrm{Si\ II}]}(\mathrm{LH}) = 0.96 \pm 0.14$, $F_{[\mathrm{S\ III}],34}(\mathrm{LL})/F_{[\mathrm{S\ III}],34}(\mathrm{LH}) = 0.92 \pm 0.20$, and $F_{[\mathrm{S\ III}],19}(\mathrm{LL})/F_{[\mathrm{S\ III}],19}(\mathrm{SH}) = 1.05 \pm 0.21$ (for targets with line fluxes above 6 σ).

2.4. *Measurements*

The $S(0)$ to $S(3)$ rotational transitions of H_2 (Table 1) were measured for all targets. In addition, we measured the $S(4)$ to $S(7)$ transitions in three galaxies in which these lines are bright enough to become detectable at low spectral resolution (see Table 3).

In high spectral resolution data, we defined errors from fluctuations of the pseudocontinuum, which was fitted as an affine function of wavelength ($F_\nu = a\lambda + b$). In SL data, errors at each wavelength were estimated from spatial fluctuations of blank fields within the satellite spectral maps that are automatically obtained when the source lies in the other half of the slit (see Smith et al. 2004). Both the fluxes and the errors presented in Table 3 were then added linearly for each point of the line profile above the pseudocontinuum. The line profiles were constrained to have a width compatible with the spectral resolution, since the latter is sufficiently low that no line is resolved. Figure 2 shows the line spectra for the representative galaxies NGC 1097, NGC 6946, NGC 7552, NGC 1266, NGC 4569, and NGC 4579.

The $S(1)$ line is usually the brightest. Of the nondwarf galaxies of the SINGS sample (with stellar masses estimated as by Lee et al. [2006] above $10^{9.5}\ M_\odot$), the nuclear regions of 86% are securely detected in the $S(1)$ line, with fluxes above 3 times the measured error. The other 14% are either ellipticals of the LINER type or late-type spirals (Sc–Sd).

There are two galaxies in common between this sample and that of Rigopoulou et al. (2002), namely, NGC 7552 and NGC 6946, the latter from the study of Valentijn et al. (1996). For both, our aperture is larger than the beam of *ISO* SWS, which covered an area of 280–380 arcsec^2. For the lines that were detected with SWS, we obtain fluxes that are higher by factors of 2.3 [$S(1)$ in NGC 6946], 5.6 [$S(0)$ in NGC 6946], and 1.1 [$S(1)$ and $S(3)$ in NGC 7552]. The exact placement of the *ISO* SWS beam is not

TABLE 3
FLUXES

Galaxy	$S(0)$ (10^{-18} W m^{-2})	$S(1)$ (10^{-18} W m^{-2})	$S(2)$ (10^{-18} W m^{-2})	$S(3)$ (10^{-18} W m^{-2})	[Si II] (10^{-18} W m^{-2})	$F_{7.9,\mathrm{dust}}$ (Jy)	F_{24} (Jy)	TIR (10^{-15} W m^{-2})
N24	6.6 ± 2.6	2.2 ± 2.4	3.2 ± 2.0	10.3 ± 6.4	36.7 ± 3.6	0.010	0.010	18.0 ± 3.0
N337	11.6 ± 3.8	21.0 ± 4.9	15.4 ± 9.9	9.7 ± 5.2	186.1 ± 7.0	0.048	0.087	89.0 ± 9.0
N628	7.9 ± 2.5	13.7 ± 5.3	0.0 ± 3.0	5.7 ± 8.6	47.8 ± 2.8	0.026	0.026	39.0 ± 3.0
N855	2.9 ± 0.9	11.2 ± 6.5	0.0 ± 5.1	22.4 ± 7.2	70.2 ± 3.8	0.017	0.039	53.0 ± 7.0
N925	3.8 ± 1.7	7.8 ± 2.9	3.7 ± 2.1	0.0 ± 8.8	81.0 ± 4.5	0.021	0.022	37.0 ± 4.0
N1097	213.1 ± 42.6	726.1 ± 43.3	293.6 ± 29.4	423.0 ± 23.4	4921.1 ± 121.9	1.139	3.763	2214.0 ± 227.0
N1266[a]	16.4 ± 8.5	148.5 ± 6.6	121.8 ± 7.1	189.8 ± 11.6	153.5 ± 41.5	0.048	0.579	438.0 ± 30.0
N1291	3.7 ± 1.8	29.8 ± 4.8	13.9 ± 8.2	31.6 ± 10.0	75.1 ± 5.8	0.013	0.049	60.0 ± 7.0
N1316	1.5 ± 0.8	36.0 ± 6.1	18.4 ± 5.9	84.0 ± 9.9	102.4 ± 6.4	0.025	0.094	105.0 ± 11.0

NOTES.—See §§ 2.2 and 2.4. For NGC 1266, NGC 4569, and NGC 4579, it was possible to measure higher level transitions of H_2, which are provided in the following notes. Table 3 is published in its entirety in the electronic edition of the *Astrophysical Journal*. A portion is shown here for guidance regarding its form and content.

[a] The $S(4)$ to $S(7)$ line fluxes are, respectively, $(102.7 \pm 17.4) \times 10^{-18}$, $(241.9 \pm 19.9) \times 10^{-18}$, $>18.5 \times 10^{-18}$, and $(192.2 \pm 28.6) \times 10^{-18}$ W m^{-2}. The $S(6)$ transition was not accurately measurable because it was observed at low spectral resolution on the blue shoulder of a bright 6.2 μm aromatic band.

known. For NGC 6946, given this uncertainty, it is conceivable that the H_2 emission be twice as bright in our 800 arcsec^2 aperture as in the SWS aperture, but the $S(0)$ line flux of Valentijn et al. (1996) is inconsistent with our data.

For this study, we estimate total infrared fluxes (TIR) between 3 and 1100 μm, defined as a linear combination of 24, 71, and 156 μm flux densities. The formula of Dale & Helou (2002) is used here, and we have checked that replacing it with the more recent prescription by Draine & Li (2007) does not change the following results in any appreciable way. The infrared fluxes are measured within the same area as the other quantities for direct comparison. The PSF width at 156 μm is, however, much larger than the size of our spectroscopic aperture, so that some extrapolation is needed. We first measure MIPS fluxes within the larger aperture used to compare total infrared fluxes with line fluxes measured in the LL module. Then, we scale these fluxes by the ratio of F_{24} measured in the small aperture to F_{24} measured in the larger aperture, which is equivalent to assuming that the spectral energy distribution does not change from an area of $\approx$300 arcsec^2 to an area of $\approx$2000 arcsec^2. The associated errors are, however, expected to be small compared with the dynamic range of the quantities discussed in § 5. Simulations of the overestimation of the far-infrared fluxes caused by the extrapolation, using a simple model of a point-source starburst (with the spectral energy distribution of Mrk 33) superposed on quasi-uniform emission from low radiation field intensity regions (with the colors of the central regions of NGC 24 or NGC 2403), indicate that the effect should be in most cases of the order of 20% (when the starburst and quiescent components contribute equally at 156 μm) and in extreme cases reach a maximum of a factor of 2 (when the quiescent component dominates). Smith et al. (2007a) reached a similar conclusion (see their § 3.2).

3. EXCITATION DIAGRAMS

Excitation diagrams provide a convenient visualization of the distribution of level populations and allow first constraints on the excitation mechanisms (thermal or nonthermal) that can produce this distribution. They represent the column density in the upper level of each observed transition N_u, normalized by its statistical weight g_u, as a function of the upper level energy E_u. The flux of a transition can be written as $F = h\nu A N_u \Omega/(4\pi)$, where A is the spontaneous emission probability, $h\nu$ is the transition energy, and Ω is the beam solid angle. In the assumption of local thermodynamic equilibrium (LTE), the total column density N_{tot} can be derived from $N_u = g_u N_{\mathrm{tot}} \exp[-E_u/(kT)]/Z(T)$, where $g_u = (2I+1)(2J+1)$ is the statistical weight (with the spin number $I = 0$ for even J or para transitions and $I = 1$ for odd J or ortho transitions) and $Z(T) \sim 0.0247T/[1 - \exp(-6000\ \mathrm{K}/T)]$ is the partition function (Herbst et al. 1996), valid for $T > 40$ K.

The apparent excitation temperature can then be derived from each pair of transitions by

$$kT = (E_{u2} - E_{u1})/\ln(N_{\mathrm{u1}}/N_{\mathrm{u2}} \times g_{\mathrm{u2}}/g_{\mathrm{u1}}), \quad (1)$$

with $N_{u1}/N_{u2} = F_1/F_2 \times A_2/A_1 \times \lambda_1/\lambda_2$. Since both radiative decay and collisions with H_2 change the rotational number J by an even number, the ortho and para states are largely decoupled and should in principle be dealt with independently.

3.1. *Ortho-Para Thermalization and Departures Therefrom*

As emphasized by Burton et al. (1992), the lower rotational levels of H_2 will be in collisional equilibrium over a wide range of conditions because their critical densities are low. Figure 3 shows the critical densities of all the rotational transitions observable with the IRS instrument, as a function of temperature, computed using the functional form for the collisional de-excitation rate coefficient by H_2 given by Shull & Beckwith (1982) and the transition probabilities given by Black & Dalgarno (1976). The derived critical densities for each line are about an order of magnitude lower than those for collisions with H computed by Mandy & Martin (1993), the comparison being made at 600 K, since Mandy & Martin (1993) provide results only for high temperatures.

The integrated emission from warm H_2 in star-forming galaxies is likely to come predominantly from the densest PDRs within the beam, with densities above 10^3 cm^{-3} (Burton et al. 1992; Kaufman et al. 2006), in which case the lowest rotational levels will be thermalized. Observations of starburst galaxies with *ISO* SWS (Rigopoulou et al. 2002) and ultraluminous galaxies with *Spitzer* IRS (Higdon et al. 2006) are indeed consistent with this expectation. At first sight, the same applies to the galaxies studied here.

However, some of the excitation diagrams show departures from thermalization of ortho levels with para levels, in the sense that the apparent temperatures derived from each pair of transitions of consecutive rotational number are not monotonic as a function of upper level energy. Clear examples are NGC 1266 [$T(S0\text{-}S1) = 201 \pm 45$ K, $T(S1\text{-}S2) = 465 \pm 34$ K, and $T(S2\text{-}S3) = 347 \pm 18$ K], NGC 4254 (162 ± 9, 358 ± 59, and 259 ± 38 K), and NGC 4631 (127 ± 8, 342 ± 39, and 268 ± 25 K). Such deviations from thermalization can be explained by an ortho-to-para

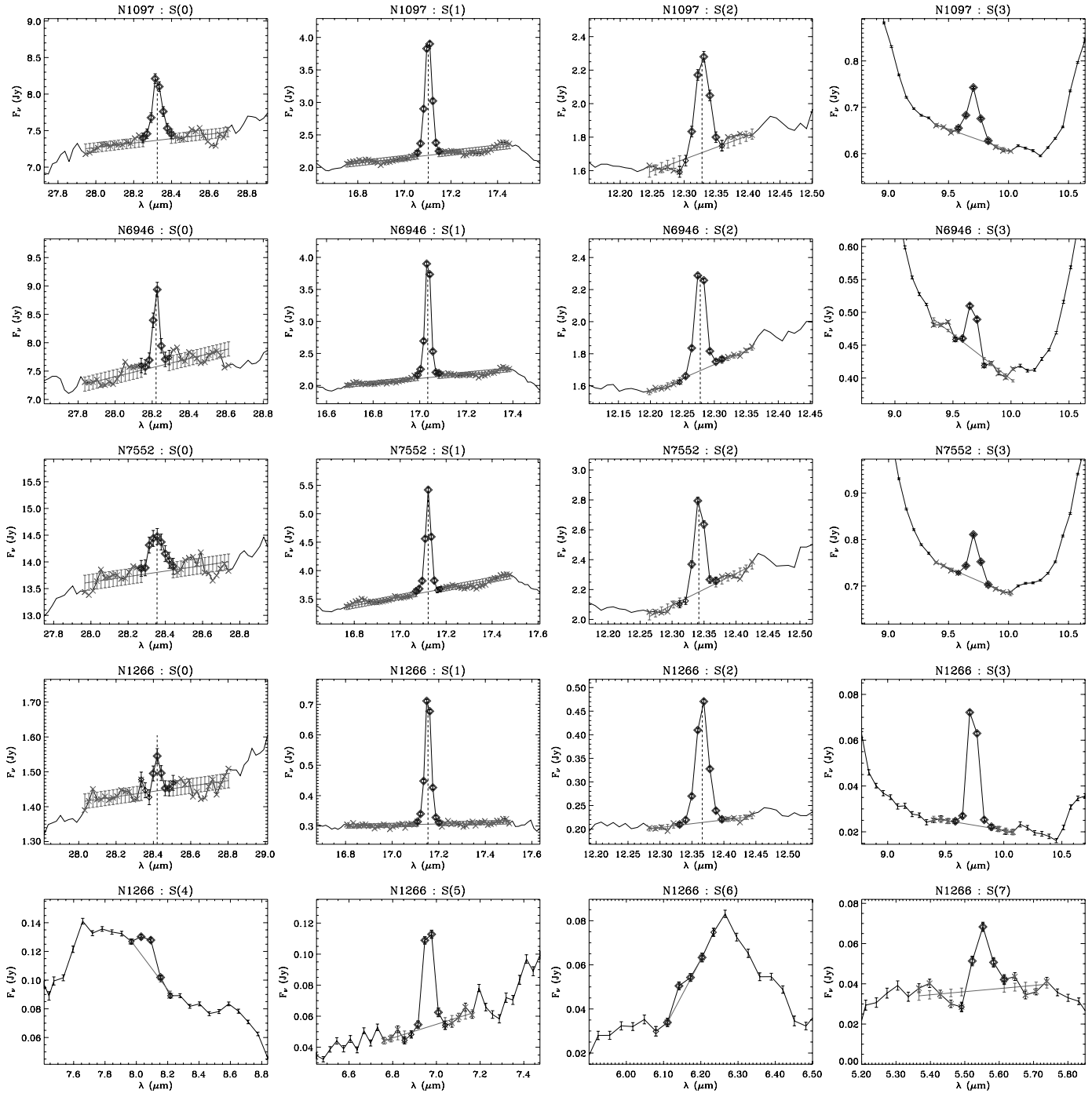

FIG. 2.—Examples of H_2 line spectra: the circumnuclear starbursts NGC 1097, NGC 6946, and NGC 7552, and the three galaxies for which we could estimate the fluxes of higher transitions than $S(3)$, NGC 1266, NGC 4569, and NGC 4579. The straight line indicates the fitted pseudocontinuum, and the diamonds show the wavelength range over which the line flux was integrated.

density ratio in the excited states apparently different from the equilibrium value. We have

$$\mathrm{OPR} = \frac{\mathrm{OPR}_{\mathrm{high}\,T}}{3}\,\frac{\sum_o (2I_o+1)(2J_o+1)\exp[-E_o/(kT)]}{\sum_p (2I_p+1)(2J_p+1)\exp[-E_p/(kT)]} = \mathrm{OPR}_{\mathrm{high}\,T}\,\frac{\sum_o (2J_o+1)\exp[-E_o/(kT)]}{\sum_p (2J_p+1)\exp[-E_p/(kT)]}, \quad (2)$$

where the subscripts o and p designate ortho and para levels, respectively ($I_p = 0$ and $I_o = 1$). $\mathrm{OPR}_{\mathrm{high}\,T}$, equal to the actual ortho-to-para ratio (OPR) in the high-temperature limit, expresses deviations from LTE if it differs from 3. It may be called the effective nuclear spin degeneracy ratio, but hereafter it is called the ortho-to-para ratio for convenience. In LTE, OPR ~ 2 for $T \sim 100$ K and OPR ~ 3 for $T > 200$ K (Burton et al. 1992), but $\mathrm{OPR}_{\mathrm{high}\,T} = 3$ at all temperatures. Although $\mathrm{OPR}_{\mathrm{high}\,T} < 3$ may be inferred for the excited states ($J \geq 2$), this does not imply that the ortho-to-para ratio of the bulk of the gas in the $J = 1$ and $J = 0$ states is out of LTE. In the following, LTE refers more particularly to the equilibrium between the ortho and para levels, and not the ortho levels or para levels separately. Extinction effects

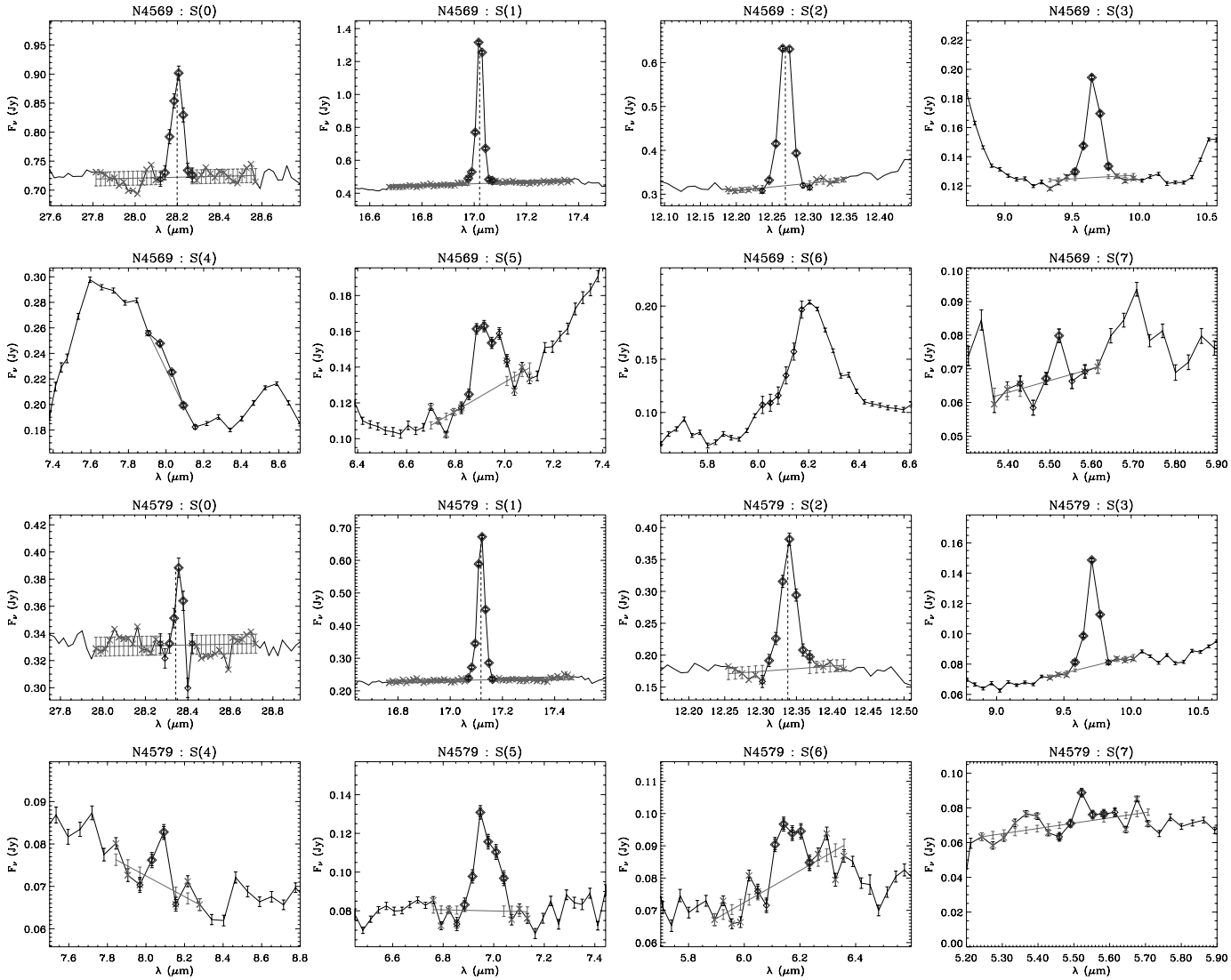

FIG. 2—*Continued*

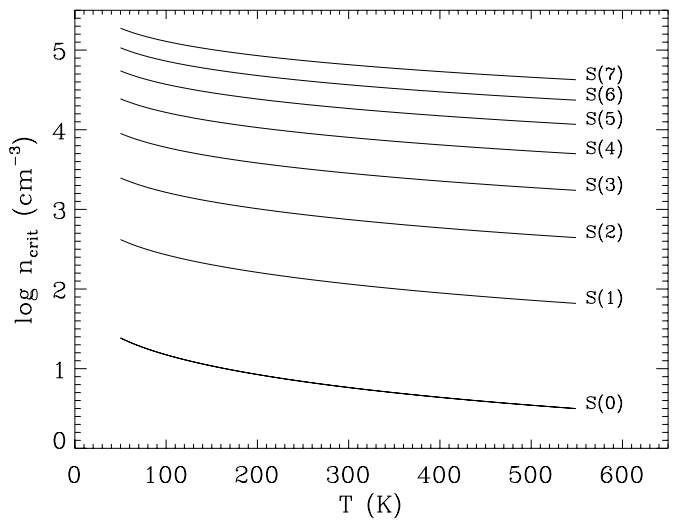

FIG. 3.—Critical densities for collisional de-excitation by H_2 for the rotational transitions in the wavelength range of the IRS instrument.

are discussed in § 3.3, and the interpretation of $\mathrm{OPR}_{\mathrm{high}\,T}$ values is postponed to § 6.

To derive temperatures and column densities, we first determine whether the excitation diagram is compatible or not with LTE by inserting explicitly the factor $\mathrm{OPR}_{\mathrm{high}\,T}/3$ in the equations for column densities of the ortho levels and deriving temperatures from each pair of consecutive transitions as a function of $\mathrm{OPR}_{\mathrm{high}\,T}$, to verify whether these conditions are satisfied: $T(S0\text{-}S1) \leq T(S0\text{-}S2) \leq T(S1\text{-}S2) \leq T(S1\text{-}S3) \leq T(S2\text{-}S3)$, since in gas with a distribution of temperatures, ratios of transitions with low-energy upper levels always probe lower excitation temperatures than ratios of transitions with higher energy upper levels. $T(S0\text{-}S2)$ and $T(S1\text{-}S3)$ are independent of $\mathrm{OPR}_{\mathrm{high}\,T}$ and determined directly from the observed fluxes, but $T(S0\text{-}S1)$, $T(S1\text{-}S2)$, and $T(S2\text{-}S3)$ depend on $\mathrm{OPR}_{\mathrm{high}\,T}$. For each pair $(p, o) = (0, 1)$, (2, 1), and (2, 3), we have

$$kT\left(S_p - S_o\right) = \left(E_{u,o} - E_{u,p}\right)/\ln\left(\mathrm{OPR}_{\mathrm{high}\,T} R\right), \qquad (3)$$

with $R = F_p/F_o \times A_o/A_p \times \lambda_p/\lambda_o \times (2J_o + 1)/(2J_p + 1)$. Figure 4 shows the corresponding diagram for two galaxies. In case the above condition on the temperatures is satisfied for $\mathrm{OPR}_{\mathrm{high}\,T} = 3$, as illustrated for NGC 3198, we fix $\mathrm{OPR}_{\mathrm{high}\,T} = 3$; in the opposite

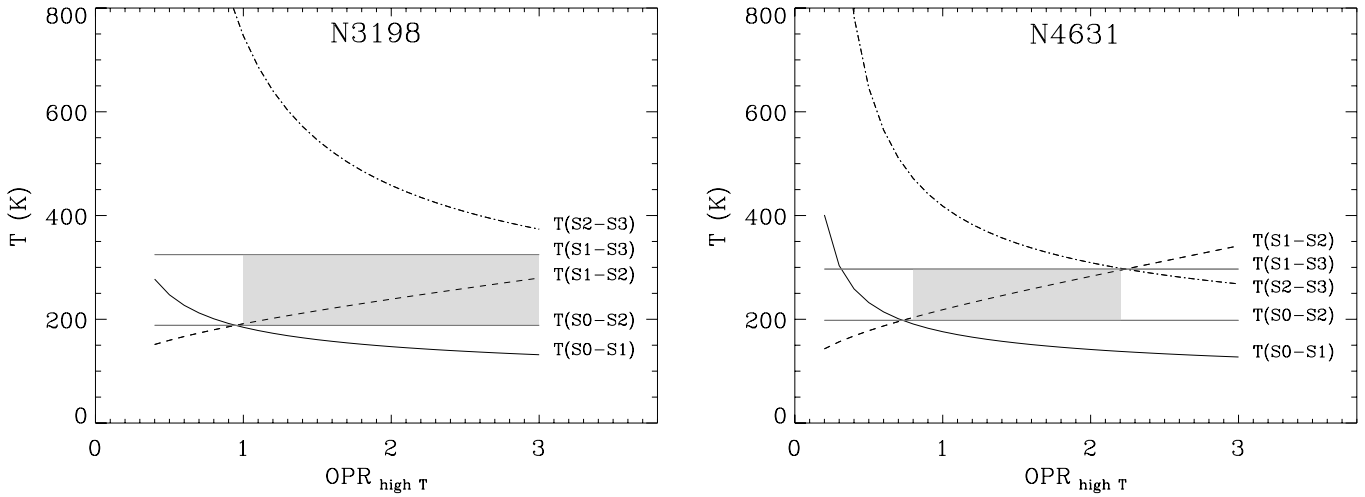

FIG. 4.—Examples of how the possible range of apparent $OPR_{high\ T}$ is determined for each galaxy. Thermalization requires the apparent temperatures derived from each pair of transitions to be monotonic as a function of upper level energy; in particular, the conditions $T(S1\text{-}S2) < T(S1\text{-}S3) < T(S2\text{-}S3)$ (indicated by the shaded areas) have to be satisfied. The apparent temperatures derived for NGC 3198 are compatible with $OPR_{high\ T} = 3$, whereas they require $OPR_{high\ T} < 3$ for NGC 4631 (see text).

case, illustrated by NGC 4631, we fit $OPR_{high\ T}$ as explained below. The excitation diagrams of all the galaxies, with fits overlaid, are shown in Figure 5.

3.2. *Temperatures and Column Densities*

Since in all cases the excitation diagrams indicate that a single temperature does not fit all the line fluxes, we assume that the H_2 emission is the sum of two discrete components of different temperatures, which is enough to reproduce accurately the observed fluxes. In the general case of $OPR_{high\ T} = 3$, we perform a least-squares fit of the excitation diagram to determine the parameters of the two discrete components (the lower temperature T_1, the upper temperature T_2, and their mass fraction) and the normalization by the total column density. The results are listed in Table 4.

When the gas is at a range of temperatures, it is in practice impossible to lift the degeneracy between mass and temperature from the lowest energy levels. Since the column density has a very steep dependence on T_1, we adopt two different procedures to fit the excitation diagrams and ascertain the amplitude of the uncertainties caused by this degeneracy. In the first case, we constrain T_1 to exceed the value for which the column density is 20% higher than the nominal density derived from $T(S0\text{-}S1)$. In the second case, we leave T_1 unconstrained. In the following, both approaches are retained when discussing results that depend on T_1.

For the results not to be biased by systematic sensitivity differences at the wavelengths of the H_2 transitions, we also replace the measured errors by a uniform weight. When $OPR_{high\ T}$ is allowed to be fitted, we fix T_2 at $1.3T(S1\text{-}S3)$ in the constrained-T_1 fits, which was chosen from the median value of T_2 in galaxies with $OPR_{high\ T} = 3$. In free-T_1 fits with $OPR_{high\ T} = 3$, the distribution of $T_2/T(S1\text{-}S3)$ is large, with a tail of high values; therefore, T_2 is first fixed at the median value, $1.14T(S1\text{-}S3)$, and then at $1.5T(S1\text{-}S3)$, to probe the full range of most likely values. Finally, when one flux is an upper limit, we fix both T_1 at $0.98T(S0\text{-}S1)$ [which increases the total column density by a maximum of $\sim$20% with respect to that obtained with $T_1 = T(S0\text{-}S1)$ but allows a small contribution from hotter gas to the $S(0)$ and $S(1)$ lines] and T_2 as above.

For the three galaxies from which more transitions, up to $S(7)$, could be measured, the procedure is the same except that a third component has to be added. The additional parameters are T_3 and the mass fraction of the second component, and T_2 is fixed at 400 K.

Several galaxies barely satisfy the criterion on temperatures to have $OPR_{high\ T} = 3$, with $T(S1\text{-}S2) \geq 0.95T(S1\text{-}S3)$ and $T(S2\text{-}S3) \leq 1.05T(S1\text{-}S3)$. When T_1 is constrained, the quality of their fits can be improved by allowing $OPR_{high\ T}$ to vary. For these objects, we provide results with $OPR_{high\ T} < 3$. Allowing $OPR_{high\ T}$ to be smaller than the equilibrium value has the indirect consequence that the derived column densities are smaller. The amplitude of this effect is indicated in Table 4. Similarly, for NGC 1705 and NGC 4552, we provide results with $OPR_{high\ T} < 3$ and indicate the change in column density with respect to $OPR_{high\ T} = 3$, because although the $S(2)$ transition being an upper limit prevents any reliable determination of $OPR_{high\ T}$, the T_1 temperatures derived with $OPR_{high\ T} = 3$ are the two lowest of the whole sample, raising the suspicion that they might be artifacts of the constraint on $OPR_{high\ T}$. We also consider $OPR_{high\ T} < 3$ more likely for these galaxies in view of the dependence of $OPR_{high\ T}$ on H_2 brightness, discussed later in § 6.

The median T_1 temperature is 154 K when the fits are constrained (ranging between 97 and 300 K); when no constraint is applied, the median T_1 is 118 K with $T_2 = 1.14T(S1\text{-}S3)$ and 161 K with $T_2 = 1.5T(S1\text{-}S3)$. The total column densities that we obtained, averaged over kiloparsec-scale regions in galactic centers, range between 10^{19} and 2×10^{21} cm^{-2} (for constrained-T_1 fits), or 2×10^{22} cm^{-2} (for free-T_1 fits), and their medians are, respectively, 3×10^{20} and $(5\text{–}6) \times 10^{20}$ cm^{-2} (Fig. 6). This can be compared with typical column densities of resolved PDRs in the Milky Way. In the Orion Bar, column densities of H_2 warmer than 400 K, derived from rotational lines, lie between 10^{20} and 10^{21} cm^{-2} (Parmar et al. 1991; Allers et al. 2005). Note that because the Orion Bar is observed nearly edge-on, an equivalent PDR seen face-on would have lower column densities. In NGC 7023, Fuente et al. (1999) derived a total column density of 5×10^{20} cm^{-2} for H_2 warmer than 300 K. Thus, if the H_2 emission in our targets comes from similar PDRs, they must occupy in general a very large fraction of the observing beam, assuming that they do not overlap on the line of sight.

Figure 6 also shows a clear dependence of the local (nuclear) column density of warm H_2 on the total stellar mass of the host

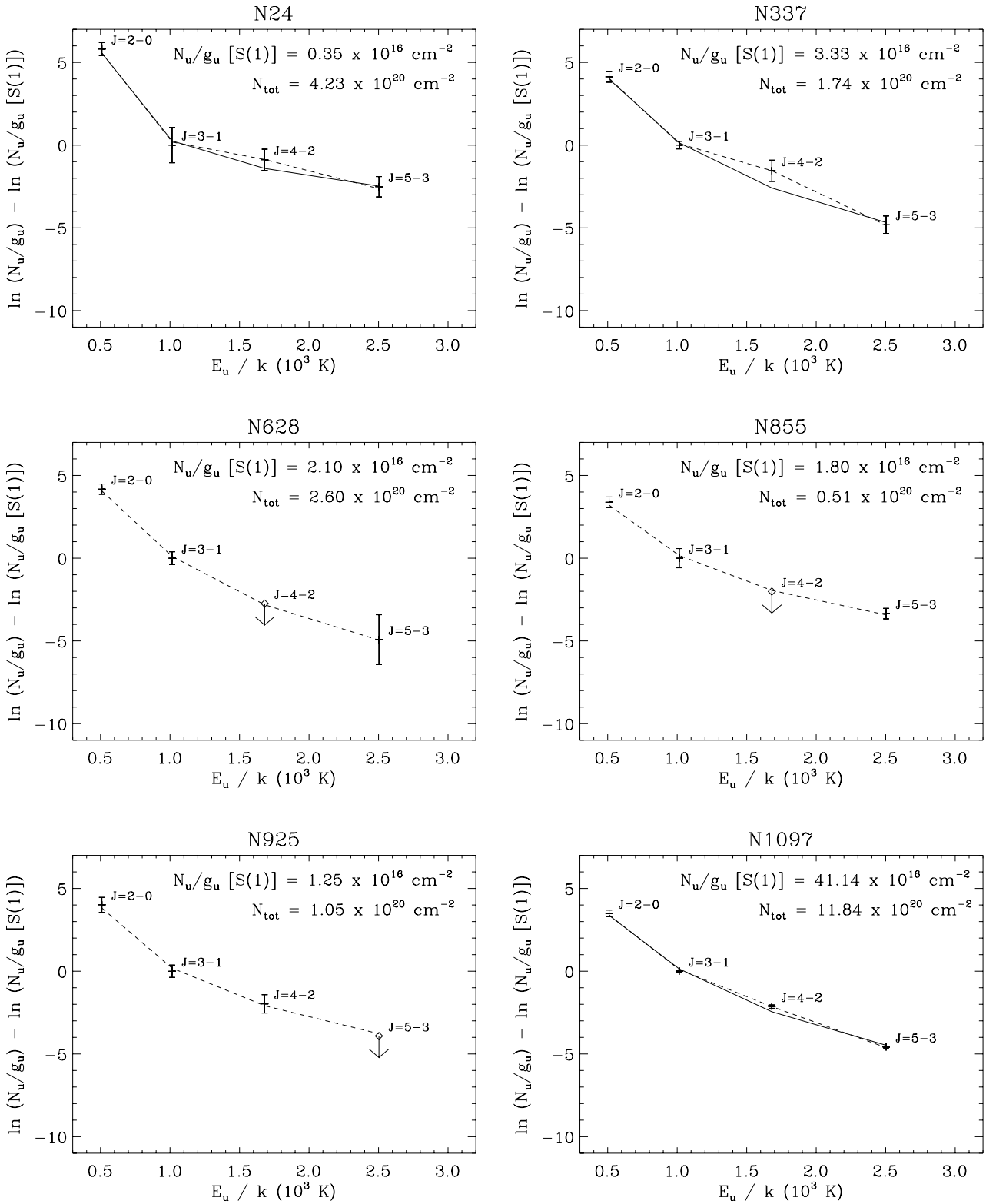

FIG. 5.—Excitation diagrams. The N_u/g_u ratios are normalized by the $S(1)$ transition. The dashed line indicates the best fit (see text). Whenever $OPR_{high\ T} < 3$ is required by the temperature constraints, a solid line shows for comparison the fit obtained with $OPR_{high\ T} = 3$. [*See the electronic edition of the Journal for additional panels of this figure.*]

galaxy. The stellar mass and the infrared luminosity being correlated for star-forming galaxies, there is a similar dependence on far-infrared luminosities. To first order, the column density of warm H_2 shows the same behavior as tracers of molecular gas and star formation rate densities, which suggests that the primary source of H_2 heating is the star formation activity in non-AGN galaxies, and the nuclear regions respond to the global mass and luminosity. LINER and Seyfert nuclei do not follow the correlation shown by star-forming regions and tend to have smaller column densities of warm H_2. The differences in terms of energy output and excitation mechanisms are studied in more detail in §§ 5, 6, and 7. Since the few extranuclear regions and dwarf galaxies included in the

TABLE 4
Derived Temperatures, Column Densities, and $OPR_{high\ T}$

Galaxy	T_1 (K)	f_1	T_2 (K)	f_2	$OPR_{high\ T}$	$N_{tot}(T > T_1)$ (10^{20} mol cm^{-2})	$N_{tot}(OPR = 3)/N_{tot}(OPR < 3)$
N24	97.0	0.99941	769.0	0.00059	1.49 ± 0.91	4.232	1.75
	78.0	0.99980	675.0	0.00020	1.90 ± 0.57	15.210	1.46
	90.0	0.99971	888.0	0.00029	1.45 ± 0.37	7.314	1.73
N337	160.0	0.97793	402.0	0.02207	1.02 ± 0.15	1.745	2.13
	128.0	0.97803	352.0	0.02197	1.21 ± 0.25	3.218	0.97
	165.0	0.98711	464.0	0.01289	0.86 ± 0.14	1.824	2.19
N628	119.0	0.99678	393.0	0.00322	3	2.598	...
N855	146.0	0.98750	578.0	0.01250	3	0.508	...
N925	123.0	0.99473	494.0	0.00527	3	1.050	...
	99.0	0.99648	421.0	0.00352	3	2.780	...

Notes.—The parameters f_i are the mass fractions of the discrete components at the temperatures T_i. For each galaxy, the first line gives the results of the fits where T_1 is constrained in order not to overestimate the column density, and the second (third) line where T_1 is unrestricted. For galaxies where the $S(2)$ flux is an upper limit, only constrained-T_1 fits were performed. When $OPR_{high\ T} < 3$, T_2 is fixed, and the free-T_1 fit results are then provided for two different values of T_2: $1.14T(S1\text{-}S3)$ (second line) and $1.5T(S1\text{-}S3)$ (third line). See § 3.2 for explanations. Table 4 is published in its entirety in the electronic edition of the *Astrophysical Journal*. A portion is shown here for guidance regarding its form and content.

sample do not distinguish themselves from the other star-forming targets in any obvious way, here and in the following, they are not discussed as separate categories.

3.3. *Optical Depth toward* H_2

Consistent with the negligible optical depths inferred from the silicate absorption bands at 10 and 18 μm in most SINGS galaxies (Smith et al. 2007a) that support the modest values of nebular extinction derived from the Balmer decrement (Dale et al. 2006), we assume zero extinction both in the lines and in the dust continuum for all the targets. In eight galactic centers among the SINGS sample (included here), Smith et al. (2007a) obtained a better fit in their decomposition of the low spectral resolution spectra by including a finite optical depth in the silicate bands. We expect the warm H_2 component to suffer less extinction, on average, than the warm dust continuum because the two emission sources will not be cospatial in general, and the regions of high optical depth will be confined to compact regions, probably more concentrated than the regions participating in H_2 emission (see the striking example of NGC 1377; Roussel et al. 2006). In particular, Higdon et al. (2006) did not see any evidence for significant extinction in the rotational H_2 lines of ultraluminous galaxies, although these objects are expected to have much higher optical depths than the present sample. In the absence of any quantitative constraint on the differential extinction between the dust and H_2, we do not attempt to correct H_2 fluxes for extinction.

Using the extinction law of Moneti et al. (2001) valid for the Galactic center, we have $A(9.7\ \mu m)/A_V = 0.15$, $A(28.2\ \mu m)/A(9.7\ \mu m) = 0.25$, and $A(17.0\ \mu m)/A(9.7\ \mu m) = A(12.3\ \mu m)/A(9.7\ \mu m) = 0.46$. Even assuming the same optical depth toward the warm molecular hydrogen as toward the hot dust, the extinction correction would not change significantly the derived column densities. The extinction is modest at 10 μm, and therefore negligible at 28 μm, the wavelength of the $S(0)$ line that dominates the total column density determination. Extinction effects would, however, depress the $S(1)$ and $S(3)$ line fluxes with respect to $S(0)$ and $S(2)$ and could thus artificially lower the derived $OPR_{high\ T}$. In the following, we put lower limits to $OPR_{high\ T}$ values, when less than 3, derived for the eight galaxies with nonzero optical depth at 10 μm.

NGC 3198 is the sample galaxy with the highest optical depth in the silicate feature according to Smith et al. (2007a), but its

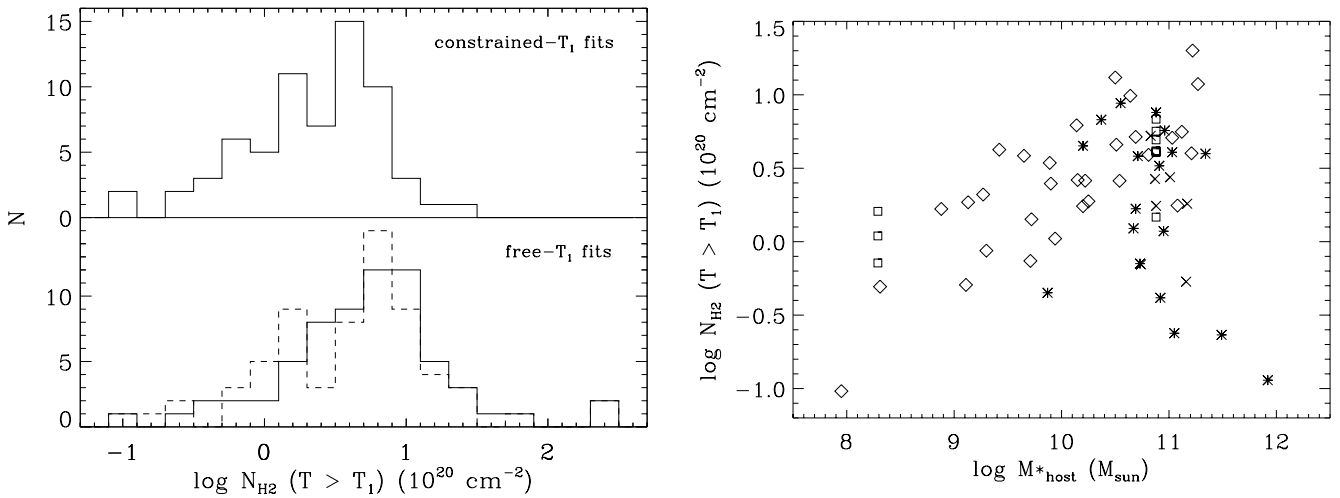

Fig. 6.—*Left*: Histograms of the derived column densities in fits where the lower temperature is constrained (*top*) and where it is free to vary (*bottom*). In the latter case, the solid line indicates results with low T_2 values and the dashed line with high T_2 values, in $OPR_{high\ T} < 3$ fits (see text). *Right*: Column densities as a function of the total stellar mass of the host galaxy, as estimated by Lee et al. (2006). Star-forming nuclei are represented as diamonds, the extranuclear regions in NGC 5194 and NGC 6822 as squares, LINER nuclei as stars, and Seyfert nuclei as crosses. By definition, dwarf galaxies have $M^*_{host} < 10^{9.7}\ M_\odot$.

TABLE 5
MASSES IN THE WARM AND COLD PHASES

Galaxy	$M(T > T_1)$ ($10^6\ M_\odot$)	N_{tot}(cold H_2) (10^{20} mol cm^{-2})	$M(T > T_1)/M$(cold H_2)	CO Beam (arcsec^2)	Corr.	Map	CO References
N24.....	3.13	...	...	...	...	...	...
N337.....	11.61	9.4	0.18	1521.0	1.52	IRAC	E96
N628.....	3.79	10.5	0.25	627.0	1.04	BIMA	S05 (B93, Y95)
N855.....	0.50	2.3	0.22	415.0	1.24	IRAC	W95
N925.....	1.15	<18.7	>0.06	386.0	...	...	S05
N1097.....	103.01	183.	0.06	1590.0	1.74	IRAC	Y95 (VV98, H93, K03)
N1266.....	12.97	...	...	...	...	...	...
N1291.....	0.42	11.7	0.04	1452.0	2.33	IRAC	T91
N1316.....	0.85	19.9	0.006	1452.0	2.55	IRAC	H01
N1482.....	73.91	136.	0.04	1521.0	1.76	IRAC	E96

NOTES.—We retain here results from constrained-T_1 fits, giving lower masses in the warm phase. Whenever the excitation diagrams are ambiguous regarding the value of $OPR_{high\ T}$, we adopt the mass of warm H_2 derived with $OPR_{high\ T} < 3$, which is also smaller than the mass derived with $OPR_{high\ T} = 3$ (see Table 4). References for CO intensities are given in abbreviated form. The quantity "Corr." designates the factor that was applied to the CO brightness in order to correct for the different apertures of the CO and H_2 observations, and "Map" is the image used to derive this factor (see § 4). Table 5 is published in its entirety in the electronic edition of the *Astrophysical Journal*. A portion is shown here for guidance regarding its form and content.

REFERENCES.—(B93) Braine et al. 1993; (E96) Elfhag et al. 1996; (H93) Helfer & Blitz 1993; (H01) Horellou et al. 2001; (K03) Kohno et al. 2003; (S05) Sheth et al. 2005; (T91) Tacconi et al. 1991; (VV98) Vila-Vilaró et al. 1998; (W95) Wiklind et al. 1995; (Y05) Young et al. 1995.

excitation diagram shows no sign of attenuation of the $S(1)$ and $S(3)$ lines relative to the others and is consistent with $OPR_{high\ T} = 3$ (Fig. 4). The second most obscured galaxy of the present sample is NGC 1266 (it also has the highest nebular extinction according to Dale et al. [2006]: $A_V = 4.1$ mag), for which we derive $OPR_{high\ T} < 3$. If this were due to optical depth effects, then the $S(3)$ line at 9.7 μm should be more attenuated than the $S(1)$ line at 17.0 μm. Since this would be consistent with the excitation diagram, we cannot exclude that the apparently low $OPR_{high\ T}$ value is an extinction artifact in at least this galaxy. The dissimilar behavior of the two galaxies in terms of differential extinction between H_2 and the dust could then arise from different excitation mechanisms and geometries: whereas in the nuclear regions of NGC 3198, classified as purely H II, the H_2 emission is presumably distributed over a large volume, the H_2 emission in the LINER nucleus of NGC 1266 may be much more compact and not produced by star formation processes (see § 5). For 13 galaxies with negligible silicate extinction in the spectral decomposition performed by Smith et al. (2007a) the excitation diagrams do imply $OPR_{high\ T} < 3$, whether a constraint on the lower temperature T_1 is applied or not. In addition, of the six galaxies found to have nonzero silicate extinction and $OPR_{high\ T} < 3$, three would require $\tau(H_2) > \tau_{sil}$ in order to obtain $OPR_{high\ T} = 3$ after extinction correction (by $\geq$25% for NGC 1266, by a factor $\geq$6 for NGC 4631, and by a factor $\geq$3.5 for NGC 5866). The three others (NGC 1482, NGC 4536, and NGC 6946) would require either $\tau(H_2) > \tau_{sil}$ or very low T_1 temperatures ($\leq$100 K). Since it is unlikely that the optical depth toward H_2 is higher than toward the dust continuum, we conclude that our finding, discussed in § 6, is robust against extinction effects.

4. MASS FRACTION IN THE WARM PHASE

In order to estimate the fraction of molecular hydrogen that is heated to temperatures above $\sim$100 K, we searched the literature for observed intensities of the 2.6 mm CO(1–0) line within a beam comparable to the solid angle of our observations. Table 5 summarizes the adopted data. The column density of cold H_2 as given here is derived from CO velocity-integrated intensities on the main-beam temperature scale, assuming a uniform conversion factor of CO(1–0) intensities to H_2 column densities of 2.3×10^{20} cm^{-2} (K km s^{-1})$^{-1}$ (Strong et al. 1988). We derived aperture corrections to the CO intensities by projecting on a map both the IRS beam and the CO beam. We did not use any deconvolution technique. Whenever possible, a map from the BIMA SONG interferometric survey, including the zero-spacing total intensity (Helfer et al. 2003), was used. Otherwise, we used instead the 7.9 μm map and assumed the spatial distributions of aromatic bands in emission and CO(1–0) line emission to be similar at the large spatial scales corresponding to our apertures. This can be justified qualitatively by the association of dust with molecular gas and the Schmidt law (for a recent study of the spatially resolved Schmidt law see Kennicutt et al. 2007). The applied correction factors are listed in Table 5. In some cases, there are several available measurements all giving consistent estimates to within 30%; the corresponding unused references are given within parentheses.

There are two major sources of uncertainty in this comparison. The first one is inherent to the difficulty of matching the physical area covered by the IRS integral-field measurements, from single-dish or aperture synthesis measurements within a different beam. The second dominant source of uncertainty comes from the conversion factor of CO intensities to H_2 masses, assumed uniform here. The result of Strong et al. (1988) is derived from a comparison of Galactic γ-ray emission with CO and H I emission. Dame et al. (2001) obtained a consistent conversion factor by extrapolating the gas-to-dust mass ratio measured from H I and far-infrared emission, in areas devoid of CO emission, to molecular clouds. Both methods provide an estimate of the total H_2 column density, including the warm gas and the cold gas, for molecular clouds under similar average physical conditions as Galactic clouds. Note, however, that conversion factors both significantly lower and significantly higher have been derived for normal galaxies. For instance, the recent study of Draine et al. (2007) favors an average value of 4×10^{20} cm^{-2} (K km s^{-1})$^{-1}$, based on global gas-to-dust mass ratios in the SINGS sample. In addition, the ratio of H_2 column density to CO intensity can vary by at least a factor of 2, depending on the physical conditions of the regions emitting in CO (Maloney & Black 1988), even though our observing aperture is large enough to cover a large number of molecular clouds and dilute some of the dispersion in their physical properties. In particular, the conversion factor is expected to be lower for compact and actively star-forming regions than for more diffuse and more quiescent regions. We

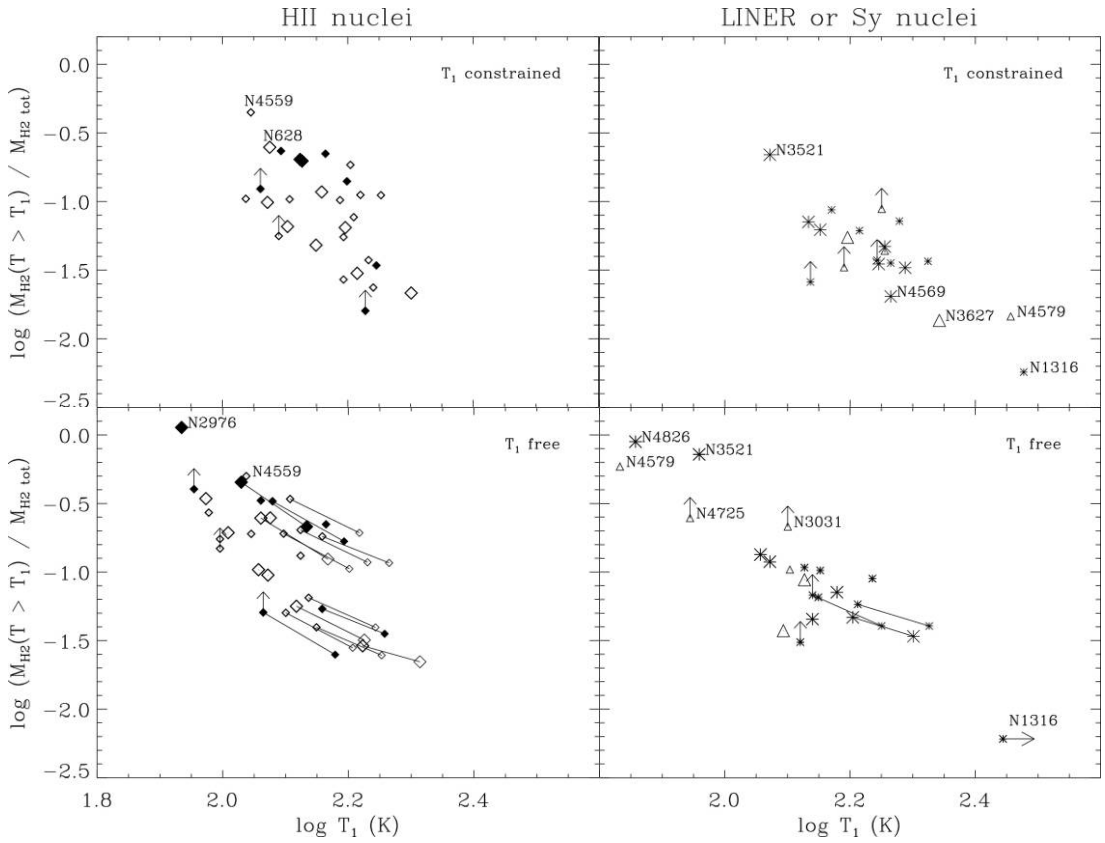

FIG. 7.—Fraction of H_2 in the warm phase ($T > T_1$) as a function of T_1, the lower temperature of the two components fitted to the rotational lines. Nuclei classified as purely star forming are shown as open diamonds, and regions in dwarf galaxies as filled diamonds; nuclei classified as LINER or Seyferts are shown as stars or triangles, respectively. The symbol size is increased for targets with the most robust CO flux estimates (see text). In the free-T_1 fits with $\mathrm{OPR}_{\mathrm{high}\ T} < 3$, results with the two values of T_2 considered here (see text) are connected by a line segment; the fits with $T_2 = 1.5T(S1\text{-}S3)$ produce higher temperatures and lower warm H_2 masses than the fits with $T_2 = 1.14T(S1\text{-}S3)$.

discount here variations due to metal abundance, since we could find CO measurements for only two low-metallicity targets (NGC 2915 and NGC 6822_A).

Figure 7 shows the mass fraction of molecular hydrogen in the warm phase ($T \geq T_1 \approx 100$ K) as a function of the minimum temperature of the warm component, as determined by the lowest energy rotational H_2 lines. The nuclei classified as star forming have a relatively narrow range of lower temperatures ($T_1 = 144 \pm 24$ K for 31 nuclei, with or without CO data, from the constrained fits). However, for nuclear regions classified as LINERs or Seyferts, the spread in temperatures is higher ($T_1 = 180 \pm 45$ K for 25 nuclei). No statistically significant difference exists between the 18 LINER and seven Seyfert nuclei.

A clear anticorrelation exists between the two quantities plotted (partly the result of the degeneracy between temperatures and column densities), which remains intact when restricting the sample to those galaxies for which we could find well-matched CO data (i.e., with correction factors close to unity and with several consistent measurements). The dynamic range in the warm gas mass fraction is much higher than accounted for by the uncertainty on the total H_2 mass. The uncertainty on the warm H_2 mass for individual objects is, however, extremely large, owing to the degeneracy between T_1, often ill constrained by the data, and the column density. The example of NGC 4579 is the most striking (see Table 4). Since its rotational levels up to $J = 5$ are close to thermal equilibrium (at a single temperature of the order of 300–400 K), such a component at 70 K as found in the free-T_1 fit is unlikely to be real. Because the fits where T_1 is unconstrained allow mass fractions in the warm phase that are sometimes unphysical (for example, for NGC 2976 and NGC 4826), we favor the constrained fits as more plausible but emphasize that the mass distribution at low temperatures is in general unconstrained.

In the case of constrained-T_1 fits, it appears that for a small set of nuclear regions classified as LINERs or Seyferts, the warm H_2 phase consists only of a very small fraction of the total mass, but heated to higher temperatures than in regions classified as purely star forming. This behavior arises naturally if normal PDR excitation is missing, and if the hotter gas is located in a thin layer of molecular clouds or has a small filling factor. In the case of free-T_1 fits, only NGC 1316 (Fornax A) remains robustly in the part of the diagram with high T_1 and mass fraction below 3%. The average temperature is, however, still higher for LINERs and Seyferts than for H II nuclei, and the average mass fraction in the warm phase likewise lower. The reason for this difference is further discussed in § 7, addressing the excitation mechanisms.

5. COMPARISON OF THE POWERS EMITTED BY WARM H_2, [Si II], AND DUST IN STAR-FORMING REGIONS

In order to empirically quantify the importance of the H_2 rotational lines in cooling the interstellar medium of normal galaxies and to put constraints on the possible excitation mechanisms of H_2, discussed in more detail in § 6, we examine power ratios of H_2 to other tracers of the warm interstellar medium extracted from the same observations. The results presented here are independent of any fits to the excitation diagrams. Only the H II nuclei and complexes are considered, LINER and Seyfert nuclei being

separately discussed in § 7. Since the bulk of warm H_2, at the lowest rotational temperatures, emits mostly in the $S(0)$ to $S(2)$ lines, whereas the $S(3)$ line emission has a noticeably higher contribution from hotter H_2, probably indicating more mixed excitation sources (anticipating the discussion of excitation mechanisms; see § 6.1), we choose, as the most useful quantification of H_2 rotational emission in star-forming targets, the sum of the $S(0)$ to $S(2)$ lines.

5.1. *Total Infrared Emission*

In PDRs, almost all the FUV power from massive stars that does not escape is absorbed by dust and converted to infrared continuum radiation, or is absorbed by H_2. Only a very small fraction of the power absorbed by dust, of the order of 1%, is converted to photoelectrons that heat the gas and emerges as infrared lines (Tielens & Hollenbach 1985). The dominant gas coolants are the [O I] and [C II] lines at 63 and 158 μm, but mid-infrared lines, in particular [Si II] at 34.8 μm and the H_2 rotational lines, are also energetically significant. Although the transition rate coefficients of H_2 are low and the excitation energies relatively high, H_2 molecules are dominant in number.

The observed ratios of the power emitted in the sum of the $S(0)$ to $S(2)$ lines to the total dust power emitted in the infrared (TIR; see § 2.4) range between 2.5×10^{-4} and 7.5×10^{-4} for nuclear regions that are not classified as LINERs or Seyferts (Fig. 8*a*). These ratios are in agreement with predictions of the photodissociation models of Kaufman et al. (2006) for a wide variety of radiation field intensities G_0 and hydrogen densities n, but a relatively narrow range of G_0/n ratios, approximately between 0.1 and 1 with G_0 in units of 1.6×10^{-3} ergs s^{-1} cm^{-2} and n in units of cm^{-3}. Note that models predict the ratio of the H_2 line power to the FUV power (for photon energies between 6 and 13.6 eV), rather than the total infrared power. Since the intrinsic FUV flux heating the PDRs is unknown, the comparison between observations and models is here made by assuming an exact conversion of FUV photons to infrared photons. The fraction of dust heating provided by non-FUV photons can, however, be significant. Allowing for this effect would reduce the derived G_0/n ratios. The H_2 rotational line fluxes predicted by Kaufman et al. (2006) are nearly an order of magnitude higher than those from the older models of Burton et al. (1992) because of the inclusion of photoelectric heating by PAHs, a better H_2 model, and a finer numerical grid near the region of H_2 emission.

The inferred G_0/n ratios are lower than the results of Malhotra et al. (2001), who derived the physical conditions of an ensemble of bright star-forming galaxies from the [C II] and [O I] lines. They found G_0/n ratios between about 0.5 and 6, i.e., on average 5 times higher than those indicated here by the rotational H_2 lines. A possible explanation is that H_2 emission comes from cooler and denser regions than [C II] and [O I] because H_2 exists at higher optical depths inside the clouds than C^+ and O (Hollenbach & Tielens 1997). The difference in physical conditions could thus merely reflect a different spatial origin. Besides the different locations within PDRs, the two studies also deal with different regions within galaxies: the targets of Malhotra et al. (2001) were selected to have most of their line emission encompassed by the *ISO* LWS beam of 70″, whereas our apertures usually cover small fractions of the line- and dust-emitting areas. Alternatively, the observations of Malhotra et al. (2001) could reflect intrinsically different physical conditions because their sample contains galaxies on average brighter and more active than the sample used here. Their far-infrared luminosities (in the definition of Helou et al. 1988) range from 6×10^7 to 8×10^{11} $L_\odot$, with a median of 1.5×10^{10} $L_\odot$, whereas the far-infrared luminosities of the present sample range from 10^7 to 6×10^{10} $L_\odot$, with a median of 3×10^9 $L_\odot$. The median F_{60}/F_{100} ratio is also higher in the sample of Malhotra et al. (2001) (0.57) than in our sample (0.41), indicating higher radiation field intensities on average. The G_0/n ratios derived by Malhotra et al. (2001), however, do not display any clear correlation with either infrared luminosity or color. Only NGC 1482 and NGC 5713, included in both samples, allow a direct comparison of model results (we discard the LINER NGC 1266 because most of its H_2 emission is not produced by PDRs, as shown in § 7). For both sources, the H_2 line fluxes indicate consistently $G_0 \sim 4000$ and $n \sim (1\text{–}2) \times 10^4$. For NGC 1482, G_0 is in agreement with one of the two models of Malhotra et al. (2001), but n is at least 4 times higher. For NGC 5713, G_0 is 2 times higher than that of Malhotra et al. (2001) and n is at least 6 times higher. In conclusion, we favor differences in spatial origin (both within PDRs and within galaxies) as a likely cause for the different model results.

5.2. [Si II] *Line Emission*

Figure 8*b* shows the ratio of powers emitted in the H_2 rotational lines and in the [Si II] line. The dispersion in the ratio is very similar to that seen in Figure 8*a*, and the [Si II] line alone emits more power than the sum of the $S(0)$ to $S(3)$ transitions in H II nuclei. The [Si II] line has indeed been found to be the brightest mid-infrared cooling line and to scale tightly with the total infrared power in both nuclear and extranuclear regions within the SINGS sample galaxies (G. Helou et al. 2008, in preparation), with only a very slight dependence on the radiation field intensity. We have on average $F(S0\text{-}S2)/F([\text{Si II}]) = 0.3$ (ranging between 0.15 and 0.5 for nuclei) and $F([\text{Si II}])/\text{TIR} = 2 \times 10^{-3}$. Using the [Si II] line as a substitute for the total dust emission is advantageous because it is observed at about the same angular resolution as the H_2 lines, whereas estimating the total infrared power within these apertures requires a large extrapolation (because of the large width of the PSF at 70 and 160 μm), making the uncertainty on H_2/TIR relatively high. The [Si II] power predicted by the PDR model of Kaufman et al. (2006), with the same physical conditions as above, is, however, smaller than observed by a factor greater than 3, which implies either that the majority of [Si II] emission comes from H II regions in high-metallicity nuclear regions or that the fraction of silicon incorporated in dust grains is smaller than 90%.

Only the regions B and C in NGC 6822 have significantly less [Si II] emission, with respect to H_2 emission, than the nuclear regions of spiral galaxies. Their H_2 emission is also slightly overluminous with respect to the aromatic bands (Fig. 8*c*). This may not be entirely attributable to a metallicity effect, decreasing the abundances of PAHs and silicon, since region A (Hubble V) has normal flux ratios and oxygen abundances are quite uniform in NGC 6822 (Pagel et al. 1980). An alternative explanation is that additional excitation of H_2 may be provided in regions B and C, with respect to region A, by shocks in supernova remnants (see the more general discussion in § 7.2). To our knowledge, no independent evidence exists to test the existence of shocks in these regions. Chandar et al. (2000) obtained a normal H II optical line spectrum at the center of NGC 6822_C, but since their beam of 2.5 arcsec^2 is only about 1% of ours, we cannot rule out shock excitation. Finally, given the small distance of NGC 6822, the regions covered by the IRS aperture are less than 100 pc in size. Greater fluctuations around the average properties are thus not unexpected. At present, we are unable to decide which scenario is the most likely.

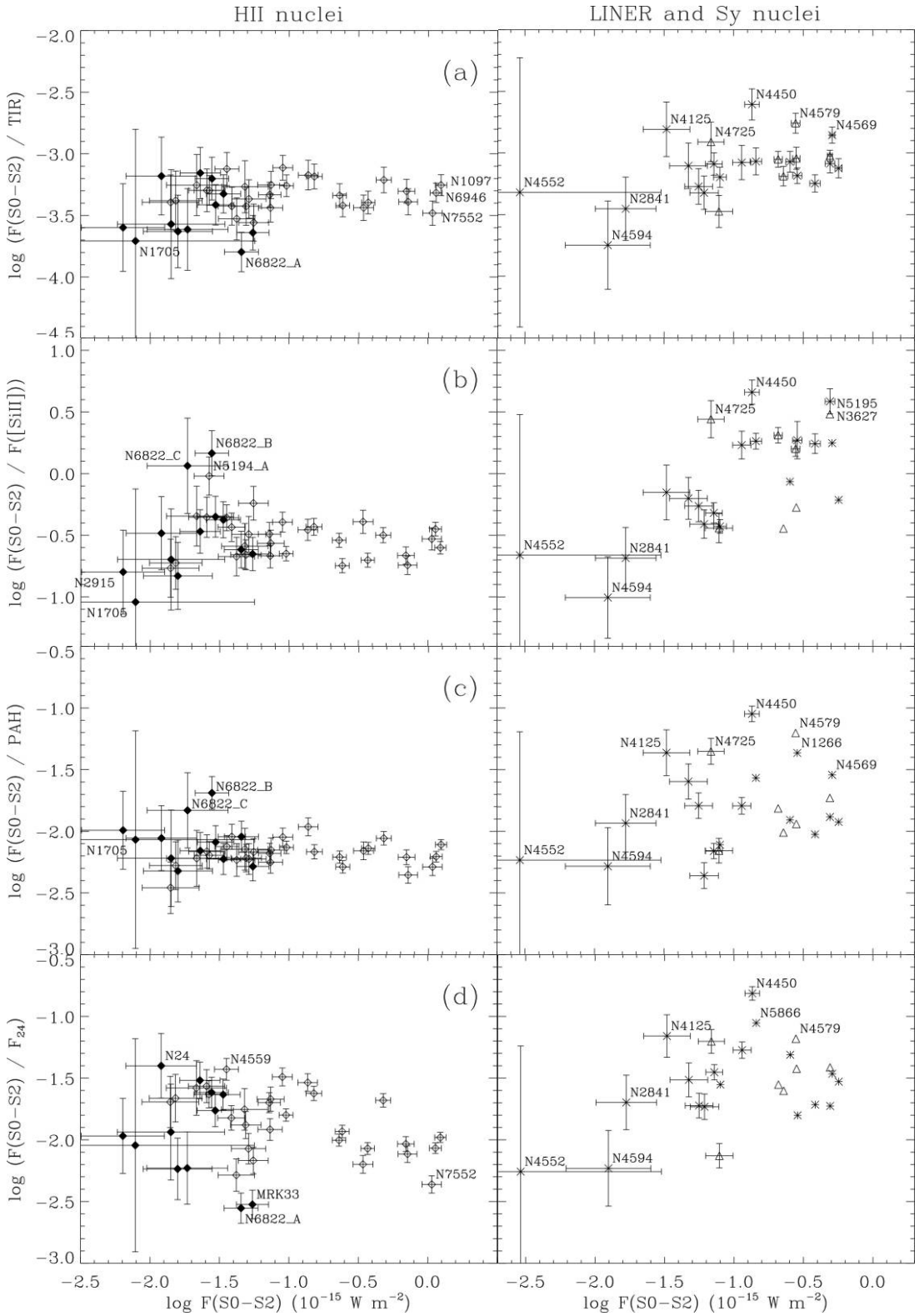

FIG. 8.—Ratio of the power emitted in the sum of the $S(0)$ to $S(2)$ transitions to (*a*) the total infrared power, (*b*) the [Si II] line power, (*c*) the power emitted in the aromatic bands within the IRAC4 filter (assuming a filter width of 13.9 THz and subtracting the stellar emission as mentioned in § 2.2), and (*d*) the power emitted at 24 μm within the MIPS1 filter (assuming a filter width of 3.1 THz). The symbol coding is as in Fig. 7. Excluding the regions within NGC 6822 (the targets with the smallest projected aperture), as well as NGC 1705 and NGC 2915 (the galaxies with the smallest H_2 brightness), the average and dispersion of each logarithmic power ratio are (*a*) -3.36 ± 0.15 for H II nuclei and complexes and -3.12 ± 0.24 for LINER and Seyfert nuclei; (*b*) -0.53 ± 0.17 and -0.04 ± 0.42, respectively; (*c*) -2.19 ± 0.10 and -1.80 ± 0.34, respectively; and (*d*) -1.85 ± 0.28 and -1.51 ± 0.31, respectively. Note that the H_2 flux (abscissa) is almost proportional to the H_2 brightness because of the quasi-uniform beam.

5.3. *Aromatic Bands*

Figure 8*c* shows a remarkable constancy of the power ratio of the H_2 rotational lines to the aromatic bands. Among the measured dust and gas observables, PAH emission provides the tightest correlation with H_2. Observations of PDRs have shown that the emission from aromatic band carriers and that from fluorescently excited H_2 just outside photoionized regions are nearly cospatial, with H_2 sometimes seen to extend slightly deeper into molecular clouds (Sellgren et al. 1990; Graham et al. 1993; Tielens et al. 1993; Brooks et al. 2000; Habart et al. 2003). Cospatiality might be expected since both species can be excited by FUV photons. Aromatic band carriers can also be excited by lower energy photons in the ultraviolet and optical, but with smaller absorption cross sections (see Li & Draine 2001), so that FUV photons will dominate the excitation whenever massive stars are present. H_2 is, however, dissociated by FUV photons between 11.3 and 13.6 eV where it is not self-shielded, whereas PAHs survive the absorption of these photons. Therefore, in the case of relatively dense PDRs (associated with molecular clouds), where collisional heating is expected to be the major origin of the H_2 rotational lines, H_2 emission should peak at slightly higher optical depth than aromatic bands, in the transition layer between atomic and molecular hydrogen, with $A_V > 1$. In addition, PAHs probably cannot be excited as deep into molecular clouds as H_2 because at sufficiently high densities they will be coagulated onto grain mantles on short timescales (Boulanger et al. 1990). If PDRs dominate the excitation of H_2, as is consistent with the above results, a tight relation between aromatic band emission and rotational H_2 emission can arise only if the physical conditions in PDRs, especially the G_0/n ratio, are relatively uniform because H_2 fluxes and PAH fluxes depend in very different ways on these two parameters. The condition of relatively constant G_0/n ratios seems verified in the present sample at least for the average emission within kiloparsec-scale regions (see above). Based on the modeling of [C II] and [O I] emission, Malhotra et al. (2001) proposed that a regulation of G_0/n might be achieved at the scale of individual PDRs by expanding H II regions in pressure equilibrium with their surrounding PDRs.

A correlation was previously claimed by Mouri et al. (1990) between the 3.3 μm band and the $v = 1{-}0$ $S(1)$ line at 2.12 μm for a small sample of starburst and Seyfert galaxies. The dominant source that they propose for H_2 excitation, following Moorwood & Oliva (1988), is, however, not PDRs, but shocks in supernova remnants. Using the shock models of Kaufman & Neufeld (1996) to estimate the sum of the $S(0)$ to $S(2)$ transitions (up to 6% of the mechanical power, assuming that its totality is dissipated in molecular clouds) and the population synthesis model of Leitherer et al. (1999) to estimate both the total mechanical power and the FUV luminosity from continuous star formation with a Salpeter initial mass function, shocks alone are in principle able to produce a significant fraction of the observed H_2 emission, but only if the efficiency of conversion of mechanical power into H_2 emission is unrealistically high. The rotational line ratios are also inconsistent with shock models, which predict higher temperatures ($T > 1000$ K) except for very low shock velocities (in which case the power fraction radiated away by rotational H_2 lines is lower). If the collective rotational line emission from shocks in supernova remnants is similar to that observed in individual objects such as 3C 391 and IC 443 (Reach et al. 2002), then this mechanism can provide only a modest fraction of the total H_2 emission. In addition, if H_2 emission came predominantly from supernova remnants whereas aromatic bands arise mostly in PDRs, the partial deconnection between the two, both temporal and spatial, would manifest itself by a large scatter in the observed relation between H_2 and PAH fluxes for galaxies with diverse star formation histories, which is not observed.

More recently, Rigopoulou et al. (2002) proposed a relation similar to that presented by Mouri et al. (1990) between the 7.7 μm aromatic band and the rotational $S(1)$ line in starburst galaxies. Figure 8*c* not only confirms this result for lower luminosity galaxies but also shows that the dispersion for the whole sample of star-forming nuclei is very small, and much smaller with the aromatic bands than with the 24 μm emission (Fig. 8*d*), which is dominated by the continuum from transiently heated very small grains, as well as from big grains in intense radiation fields. The quantification of the average H_2-to-dust power ratios and their dispersions is given in the caption of Figure 8. The energy coupling between aromatic band carriers and H_2 strongly suggests that both are excited predominantly in PDRs, although they may not come from the exact same layers (at the same optical depths within the clouds). We present further analysis in the next section.

A similar correlation, with a similarly small dispersion, was observed between the [C II] line and aromatic band emission (Helou et al. 2001). This relation suggests that aromatic band carriers are the source of a major part of gas heating in PDRs, via the photoelectric effect, at least at modest radiation field intensities, since [C II] emission is the dominant cooling channel in this case. In the narrow range of physical conditions that seem to apply if the emission from H II nuclei is interpreted in the framework of PDR models (a dynamic range in G_0/n of only a factor 10), the same link between aromatic band carriers and H_2 would follow if H_2 were heated in relatively dense PDRs by the PAHs. Our results, however, suggest that in nearly half the star-forming targets, the dominant excitation mechanism of the rotational levels may be fluorescence in low-density regions, so that ortho-para thermalization is not achieved by collisions (see § 6). If the lines are fluorescently excited, the cause underlying the tight relation between H_2 and aromatic band emission may be that both are proportional to the incident FUV flux that excited them.

5.4. *Cirrus Clouds versus PDRs with High Radiation Field Intensities*

The tight association between H_2 emission and aromatic bands (Fig. 8*c*) may be surprising if one assumes that a significant fraction of aromatic band emission arises from diffuse, mostly atomic regions with low radiation field intensities. The infrared emission of such clouds is often termed cirrus (Low et al. 1984; Terebey & Fich 1986). If this were the case, then the scaling of PAH flux with H_2 flux could be explained only if a constant fraction of the total FUV flux escaped PDRs and were absorbed in the more diffuse interstellar medium. We stress that we adopt here the definition of PDRs stated by Hollenbach & Tielens (1997): these are not restricted to the interfaces between bright H II regions and dense molecular clouds, but apply more generally to all the neutral interstellar medium illuminated by FUV photons (with energies between 6 and 13.6 eV). Figure 9 demonstrates the great difficulty of making the idea of an important contribution from the cirrus medium consistent with the data. It shows the flux ratios of H_2 to PAH emission on the one hand and 24 μm to PAH emission on the other hand, as a function of $P_{24} \sim \nu_{24}F_{24}/(\nu_{71}F_{71} + \nu_{156}F_{156})$, estimated within the spectroscopic apertures. The quantity P_{24} is closely related to $f_{U>100} = f(L_{\rm dust};\ U_{\rm rad} > 100)$, derived from the modeling of the global spectral energy distributions by Draine et al. (2007), which is the fraction of the total dust luminosity emitted by regions with radiation field intensities $U_{\rm rad}$ higher than

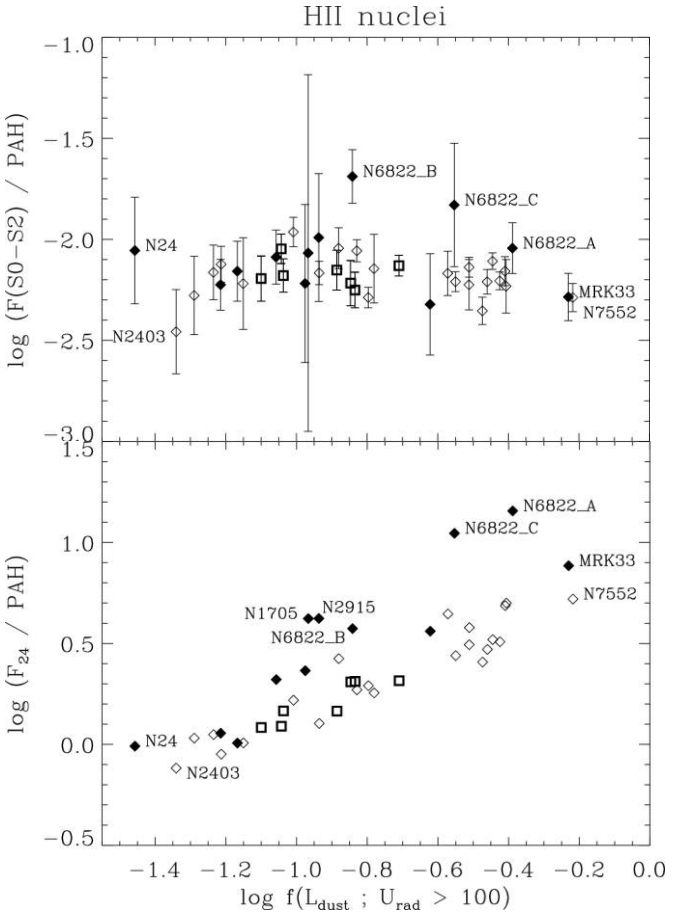

FIG. 9.—Power ratios of H_2 to aromatic bands (shown in Fig. 8*c*) and 24 μm emission to aromatic bands as a function of $P_{24} = 1.05[(\nu_{24}F_{24} - 0.14\nu_{7.9}F_{7.9,\mathrm{dust}})/(\nu_{71}F_{71} + \nu_{156}F_{156}) - 0.035]^{0.75}$, a quantity closely related to $f(L_{\mathrm{dust}}; U_{\mathrm{rad}} > 100)$ defined by Draine et al. (2007), which is the fraction of the total dust luminosity coming from regions with radiation field intensities more than 100 times the average local field. Only H II nuclei and complexes are shown. Dwarfs are represented by filled diamonds, and the extranuclear regions within NGC 5194 by thick squares.

100 times the local average value. The dust luminosity fraction of cirrus clouds, $\sim f_{U<10}$, can be evaluated as $1 - cf_{U>100}$, if one assumes that $f_{U>100}$ and $f_{U>10}$ are in constant proportion to each other. Figure 9 shows that while the F_{24}/PAH ratio rises by about 1 order of magnitude, the H_2/PAH ratio is invariant as a function of P_{24} or $f_{U>100}$. The results obtained by replacing P_{24} with F_{71}/F_{156}, which has the same physical significance as F_{60}/F_{100}, a more traditional indicator of the relative importance of H II regions and cirrus clouds (Helou 1986), are identical.

We conclude that aromatic bands are mostly associated with PDRs (illuminated by FUV photons able to provide H_2 excitation). In addition, since PAHs are excited not only by FUV photons but also by low-energy photons, the observed constancy of the H_2-to-PAH ratio imposes some restrictions on possible variations of the radiation field hardness. Assuming that cirrus clouds, i.e., PDRs with low radiation field intensities, receive appreciably softer radiation than PDRs with high radiation field intensities, it would be difficult to understand how both types of regions could produce similar H_2/PAH ratios. As a corollary, the hypothesis that cirrus clouds could make a large contribution to H_2 and PAH emission in our targets, although not definitely ruled out, is not favored. Note that the situation may be different in more quiescent parts of galaxies, not probed by the present sample, and deserves further investigation. Measurement of H_2 line fluxes in quiescent regions is, however, challenging because they depend steeply on the G_0 and n parameters.

The above does not preclude a large portion of the H_2 and PAH emission to originate in relatively diffuse molecular gas. Estimates of the optical depth of the ^{12}CO(1–0) line, over large areas of the Galaxy, indicate that the total molecular medium comprises a substantial diffuse component (Polk et al. 1988). We see in the next section that our data, for a portion of the targets, do support an important contribution from low-density PDRs to the total warm H_2 emission.

6. EXCITATION MECHANISMS IN STAR-FORMING REGIONS

In sources with purely stellar activity, H_2 emission is expected to arise in varying proportions from two main energy sources: the FUV radiation of OB stars illuminating PDRs, and shocks in supernova remnants or other sources, providing collisional heating. In the first case, the excitation can be thermal, by collisions with gas heated by photoelectrons, or by inelastic collisions with H_2 molecules pumped by FUV photons. The excitation mechanism can also be fluorescence, followed by radiative cascade to the ground vibrational state. Heating by supernova remnants is unlikely to be dominant for two reasons, as we have seen in § 5.3. First, at the low observed temperatures dominating the warm H_2 mass, heating would have to be provided by slow shocks, which are not efficient enough to compete with PDR excitation. Second, variations in star formation histories within the sample, which are shown by J. Moustakas et al. (2008, in preparation) to be very large (from population synthesis fitting to optical spectra), would produce more scatter than observed in the H_2/PAH ratio. We conclude that H_2 is heated predominantly by PDRs, and this interpretation is supported both by energetics arguments and by the close association with aromatic band emission (§ 5). In this section we focus on additional constraints on the physical conditions and excitation mechanisms in PDRs (thermal or fluorescent) from the line ratios and excitation diagrams.

6.1. *Constraints from the Temperature Distribution*

We have seen that the H_2–to–far-infrared ratios are consistent with values of G_0/n, the ratio of the average radiation field intensity to the hydrogen density in PDRs, between about 0.1 and 1. In principle, separate constraints on G_0 and on n can be obtained from the temperature distribution reflected in the H_2 line ratios (Kaufman et al. 2006). Given the complexity of the surveyed regions, however, the interpretation of the line ratios by comparison with models of a single PDR is severely limited. First, the emission from many distinct PDRs, presumably showing a large range of physical conditions, is averaged within the beam. Second, even though the total emission in the sum of the $S(0)$ to $S(3)$ lines is probably dominated by PDRs, shocks also related to the star formation activity must be present, driven in particular by supernova remnants, protostellar outflows, or turbulence dissipation (Falgarone et al. 2005). Since these shocks are characterized by higher rotational temperatures than PDRs, they would contribute mostly to the $S(3)$ line (Kaufman & Neufeld 1996) and, in view of the observed line ratios, negligibly to the lower lying transitions.

In both cases, the superposition of PDRs of different conditions or of shocks induces a spread in temperatures, and as a consequence these are not reproduced by single PDR models. We compared the line ratios of the star-forming targets with $\mathrm{OPR}_{\mathrm{high}\,T} = 3$ to the predictions of Kaufman et al. (2006). Although the ranges in G_0 and n derived from $S(2)/S(0)$ have a broad overlap with those derived from $S(1)/S(0)$, the $S(3)/S(1)$ ratios are inconsistent,

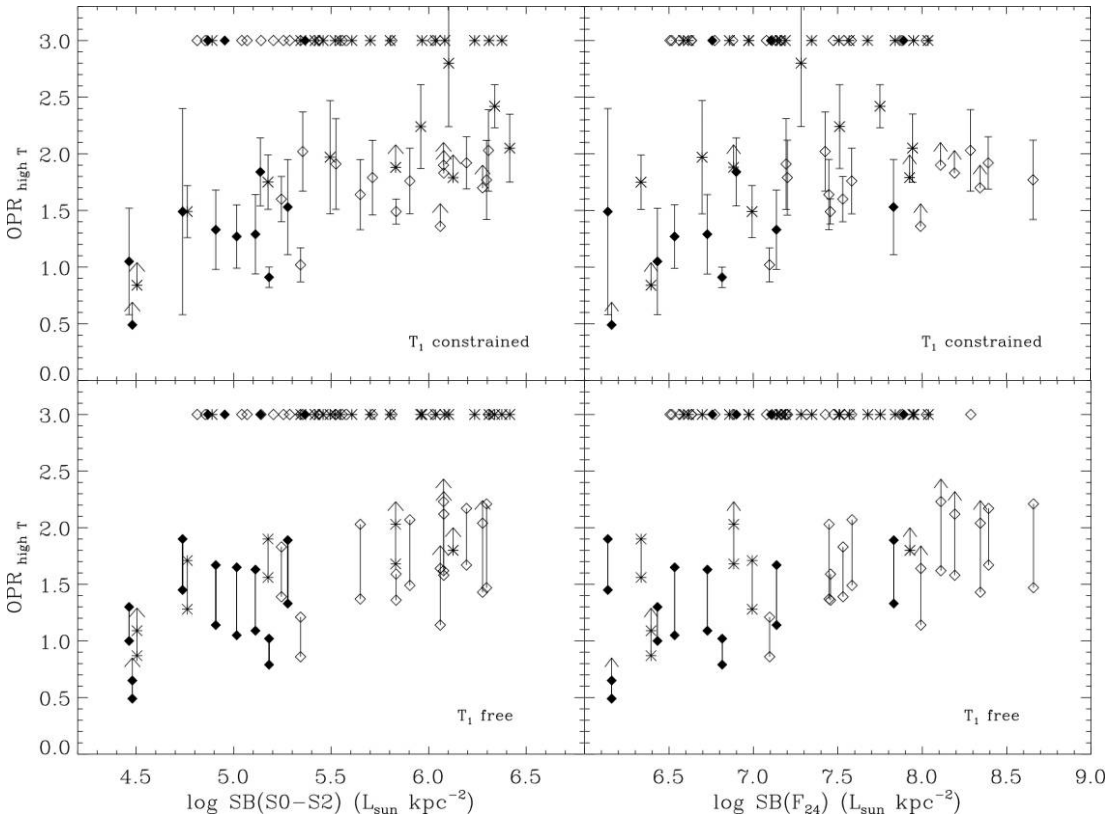

FIG. 10.—Ortho-to-para ratios as a function of the surface brightness in the sum of the $S(0)$ to $S(2)$ transitions and as a function of the surface brightness in the 24 μm band. For a number of sources, based on the excitation diagram, we adopted a fixed $OPR_{high\ T} = 3$ (see text). Galaxies with upper limits in the $S(2)$ line, or with indications of possibly nonnegligible optical depth at 10 μm, are shown as lower limits of $OPR_{high\ T}$. For free-T_1 fits, results obtained from the two values of T_2 considered here are connected by a line segment. The symbol coding is as in Fig. 7, except that LINER and Seyfert nuclei are both shown as stars.

indicating more intense radiation fields and higher densities. The least biased tracer of physical conditions in the bulk of the PDRs is thus the $S(1)/S(0)$ ratio (for galaxies with $OPR_{high\ T} = 3$). It suggests that the average G_0 varies between about 100 and 5000 (in units of 1.6×10^{-3} ergs s^{-1} cm^{-2}) and the average n between about 500 and 10^4 cm^{-3}.

6.2. *Fluorescent Excitation*

It is surprising that in several objects, the $S(0)$ to $S(3)$ transitions are not thermalized, as indicated by deviations from an apparent $OPR_{high\ T}$ of 3. OPR values that are different from the equilibrium value at the temperature of the H_2 gas arise naturally from fluorescent excitation, if the gas density is lower than the critical density for ortho-para equilibration by collisions with H and H^+ (Sternberg & Neufeld 1999). This is because the ultraviolet absorption lines have a greater optical depth in the ortho states than in the para states, so that the ortho states at a given depth are pumped less. The apparent $OPR_{high\ T}$ values only apply to the states excited by FUV pumping and do not imply that the true $OPR_{high\ T}$ value (for the $J = 1$ and $J = 0$ states, where most of the gas resides) is different from 3. For a total $OPR_{high\ T}$ of 3, the $OPR_{high\ T}$ of the excited levels is predicted to be close to $\sqrt{3} = 1.7$. A thorough review of the phenomenon of selective excitation and its implications for the interpretation of excitation diagrams was provided by Sternberg & Neufeld (1999). Note that radiative decay in the electronic ground state and most collisional (de-)excitations always occur at fixed spin number and thus preserve the ortho or para state. Conversion from one state to the other can be accomplished by H_2 dissociation followed by reformation on dust grains, or by reactions with protons and hydrogen atoms in the gas phase.

Deviations from thermalization had previously remained unseen for rotational lines of extragalactic sources (Rigopoulou et al. 2002; Higdon et al. 2006). In the frame of PDR excitation, values $OPR_{high\ T} < 3$ may be interpreted as arising in FUV-pumped gas with sufficiently low densities to prevent ortho-para equilibration by collisions. However, because this process depends on unknown timescales for gas heating, cooling, dissociation, and reformation, we are unable to quantify in a simple way the implied density conditions. Alternatively, it is conceivable that the emission comes from initially cold gas that has been heated by slow shocks and has not had time to reach the equilibrium value of OPR (Timmermann 1998; Wilgenbus et al. 2000). For H II nuclei, however, we have seen that PDR excitation is more likely than shock heating (§ 5).

Another possibility is that in a fraction of the PDRs within the beam, the photodissociation front is advancing into cold gas [in LTE at time t_1 with $OPR(t_1) \ll 3$ and $OPR_{high\ T}(t_1) = 3$], and the recently heated gas has not yet had enough time to reach LTE at time t_2 [with $OPR(t_2) \sim OPR(t_1)$ and $OPR_{high\ T}(t_2) < 3$ according to eq. (2)]. This is the interpretation favored by Fuente et al. (1999) and Habart et al. (2003) to explain the non-LTE ortho-to-para ratios observed in the PDRs of NGC 7023 and ρ Ophiuchi, respectively. In this scenario, the observed portion of the interstellar medium would have to contain a much larger fraction of nonequilibrium PDRs in targets with low $OPR_{high\ T}$ than in targets with $OPR_{high\ T} = 3$, and the underlying reason would be unclear. It is also unknown whether the timescales involved in ortho-para equilibration in our sources are long enough for this scenario to be viable.

Figure 10 shows the derived $OPR_{high\ T}$ values (fixed to 3 whenever the temperatures derived from each pair of adjacent transitions

were compatible with this assumption) as a function of the total brightness of the $S(0)$ to $S(2)$ lines. We have here included LINERs and Seyferts because they do not display a different behavior in this diagram. Under the hypothesis of PDR excitation, and assuming first that sites of star formation occupy a constant fraction of the observing beam, sources with low H_2 brightnesses should consist of regions with both low densities and low radiation field intensities, while sources with the highest H_2 brightnesses should include a greater fraction of high-density, high-radiation regions. In this simplified view, low values of $OPR_{high\ T}$, indicating that H_2 is not thermalized by collisions, could be obtained only in the low-brightness sources, as seen generally in Figure 10. Variations in the beam filling factor by sites of star formation would then induce a horizontal scatter, which is indeed very large. Figure 10 also shows $OPR_{high\ T}$ as a function of the average surface brightness in the 24 μm band. The latter quantity incorporates a significant contribution from H II regions and should be dominated by variations in radiation field intensity, rather than variations in gas density. The fact that the horizontal spread is larger in this diagram than in the diagram involving the H_2 brightness supports our tentative interpretation in terms of density effects. In addition, $OPR_{high\ T}$ does not show any variation as a function of F_{71}/F_{156}, and only a weak tendency to increase with the quantity P_{24} discussed in the previous section. Both these quantities are indicators of the average radiation field intensity; they are observed to be generally correlated with the gas density, but only weakly. Although the data do not allow us to truly estimate average densities in PDRs, they suggest that in a substantial number of the observed nuclear regions, the emission can be dominated by low-density gas, relative to well-studied Galactic PDRs and starburst galaxies. New modeling is required to quantify the conditions under which rotational lines indicate $OPR_{high\ T} < 3$ in PDRs.

The H_2 line ratios, compared with the PDR model of Kaufman et al. (2006), do not indicate lower gas densities, on average, in galaxies with $OPR_{high\ T} < 3$ than in galaxies with $OPR_{high\ T} = 3$. However, the densities estimated in this way are averages within the whole beam, and the densest and warmest regions have a greater weight because they are more luminous in H_2; if a large spread in densities exists, with both dense clumps and diffuse PDRs, an increase in the diffuse fraction may not be easily detectable in the average density, while still leaving an imprint on $OPR_{high\ T}$. We note that the proton density should also play an important role, since ortho-para conversion is effected by collisions with H and H^+. Whether galaxies with $OPR_{high\ T} < 3$ have lower proton densities in molecular clouds, due to reduced ionization by cosmic rays, is in principle testable with radio continuum observations of synchrotron radiation from cosmic-ray electrons. The number of sample galaxies with adequate data, at sufficiently high angular resolution, is, however, too small to apply this test.

We have seen in § 3.3 that extinction effects are unlikely to modify our results in a statistical sense. The fitted $OPR_{high\ T}$ values are correlated with the brightness of the dust emission, in the aromatic bands, the 24 μm continuum, and total infrared emission (not shown here but similar to Fig. 10), which is a further indirect argument against extinction effects being responsible for low $OPR_{high\ T}$ values. If extinction played a significant role, then low $OPR_{high\ T}$ values would be seen preferentially in bright and compact regions, which is not the case.

The galaxies for which we derive the lowest $OPR_{high\ T}$ values (and among the lowest H_2 surface brightnesses, regardless of the constraint on the T_1 temperature) are NGC 337, NGC 1705 ($OPR_{high\ T}$ is a lower limit), NGC 2915, NGC 4552 ($OPR_{high\ T}$ is a lower limit), and NGC 7793. The first three are dwarf galaxies, NGC 7793 is a very late-type spiral, and NGC 4552 is a small elliptical galaxy classified as LINER, with the smallest infrared brightness of the whole sample. Since smaller gas densities are expected in general in dwarf galaxies than in the central regions of massive galaxies, except in blue compact dwarfs such as Mrk 33, this finding is consistent with our interpretation of small $OPR_{high\ T}$ values in terms of low density. We may also remark that in NGC 1705, which is a starburst, no ultracompact H II region was detected in the radio (Johnson et al. 2003); thus, no conflict exists with the hypothesis that the PDRs in NGC 1705 have low densities.

7. EXCITATION MECHANISMS IN LINER AND SEYFERT NUCLEI

A large number of the galaxies classified as LINERs or Seyferts deviate significantly from the relations discussed in § 5, in having a strong excess of H_2 emission with respect to all the other tracers used here, not only aromatic bands but also [Si II], the 24 μm flux, and the total infrared emission (Fig. 8), arguing for an alternative excitation mechanism in these galaxies. The average and dispersion of each power ratio are given separately for H II nuclei and for LINER and Seyfert nuclei in the figure caption. Given these results, the quantities by which the two categories are most clearly separated are the H_2–to–aromatic band ratio and the H_2–to–[Si II] ratio. In particular, nuclear regions with $F(S0\text{-}S2)/F_{7.9,dust} > 10^{-1.94}$ are likely to be of the LINER or Seyfert type at the 99% confidence level.

We thus define an excess of H_2 emission, with respect to H II nuclei, based on the observed relation with aromatic bands. We choose as the maximal H_2 power associated purely with star formation the quantity $10^{-1.94}L_{7.9,dust}$. Aromatic band carriers are thought to be destroyed in intense radiation field environments, such as H II region cores (Giard et al. 1994) and ionized regions around Seyfert nuclei (Désert & Dennefeld 1988; Voit 1992). They would, however, survive where H_2 is not dissociated, so that an enhancement of the H_2/PAH ratio is more likely caused by a genuine excess of H_2 emission, in conditions where PAHs are not excited, rather than normal H_2 emission occurring where PAHs would have been destroyed. Furthermore, H_2 emission is seen in excess not only with respect to aromatic bands, but also with respect to [Si II] and other dust tracers (24 μm and total infrared emission). [Si II] emission may be depressed because the ionization state of silicon becomes higher, but the dust continuum cannot be suppressed like aromatic bands. Our empirical quantification of the H_2 excess is intended to extract the part of H_2 emission that cannot originate in PDRs. The excitation mechanism that is required to account for this excess, while not exciting PAHs, is either X-ray irradiation or shock heating.

We discuss LINER and Seyfert nuclei as a single category because no detectable difference exists in their H_2 properties. This may be expected for several reasons: small number statistics, the fact that the classification of low-luminosity AGNs can be ambiguous as it depends on the aperture size in particular, and the fact that the source of H_2 excitation might not be directly linked to the nuclear activity, as the results discussed below suggest.

7.1. *Heating by X-Rays from an Active Galactic Nucleus*

The idea that a nuclear X-ray source may modify the chemistry and excitation of the surrounding molecular clouds through sufficiently large column densities as to offer a convenient way to identify active nuclei hidden by dust has recently received much attention. Models predict, in particular, unusual ratios of tracers of dense molecular gas (Lepp & Dalgarno 1996; Meijerink & Spaans 2005), consistent with observations of NGC 1068 (Usero

TABLE 6
NUCLEAR X-RAY FLUXES IN THE 2–10 keV BAND AND REFERENCES

Galaxy	F_X (10^{-17} W m^{-2})	References	Note[a]
N628	0.59	K05	1
N1097	173.0	N06	2
N1291	7.45	K05	1
N1316	10.1	KF03	1
N2841	1.06	HF01	2
N3031	1020.0	HF01	2
N3184	1.12	K05	1
N3627	<0.32	HF01	2
N4125	1.07	S04	2
N4321	<1.25	HF01	2
N4552	12.1	SD05	2
N4569	7.61	HF01	2
N4579	264.0	HF01	2
N4594	120.0	HF01	2
N4725	7.15	HF01	2
N4736	27.4	SD05	2
N4826	<1.08	HF01	2
N5033	123.0	HF01	2
N5194	1300.0	S04	2
N5195	4.45	K05	1
N5866	0.18	SD05	2
N7331	2.28	S04	2

[a] (1) Quantity computed as in Ho et al. (2001) from counts in the 0.2–8 keV band. (2) Quantity given directly in the cited paper (abbreviated notation as in the list of references).

REFERENCES.—(HF01) Ho et al. 2001; (K05) Kilgard et al. 2005; (KF03) Kim & Fabbiano 2003; (N06) Nemmen et al. 2006; (S04) Satyapal et al. 2004; (SD05) Satyapal et al. 2005.

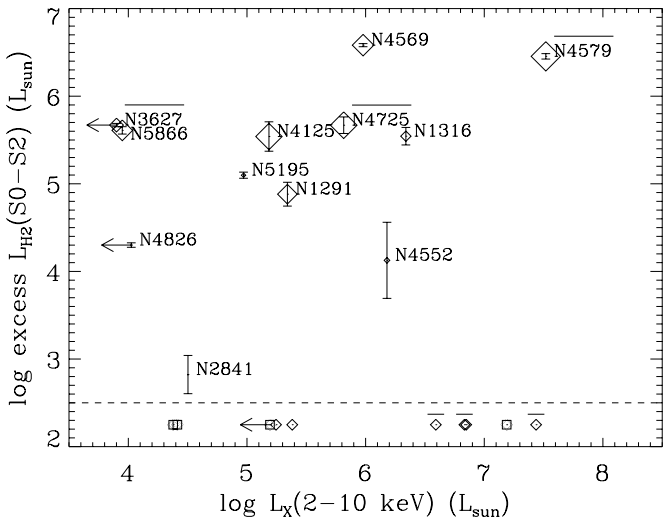

FIG. 11.—Excess H_2 luminosity as a function of 2–10 keV X-ray luminosity. The excess H_2 emission is defined from the relation between H_2 and aromatic band power, shown in Fig. 8*c*, as the difference between the total H_2 emission and the quantity $10^{-1.94}F_{7.9,\mathrm{dust}}$, which defines the upper envelope of H II nuclei. Galaxies with no H_2 excess according to this definition were arbitrarily placed at an ordinate of 2.25 below the dashed line. The size of the symbols is proportional to the fraction of excess H_2 to total H_2 emission, coded as in Fig. 12. Seyfert nuclei are marked by an overlying horizontal bar, and star-forming nuclei by a square. The large scatter and the high ratios of excess H_2 to X-ray luminosities argue against X-rays playing a dominant role in the additional (nonstellar) excitation of H_2 in LINER /Seyfert nuclei (see text).

et al. 2004). X-ray excitation would also manifest itself in the properties of H_2, the most abundant molecule. To test the hypothesis that the additional excitation in galaxies showing a significant excess of H_2 emission with respect to aromatic bands (Fig. 8*c*) is predominantly produced by nuclear X-rays, we have compiled estimated X-ray fluxes in the 2–10 keV band obtained from *Chandra* observations. The data and references are summarized in Table 6. The H_2 excess is shown as a function of the X-ray luminosity of the nucleus in Figure 11. Here galaxies with no H_2 excess according to our definition are shown below the dashed line.

The spread in Figure 11 is very large. Since the available X-ray measurements do not isolate the hard X-ray component, but include soft emission, a substantial part can be thermal emission from supernova remnants, as opposed to power-law emission from the activity related to a central supermassive black hole. Many H II nuclei with no H_2 excess indeed have X-ray luminosities that are comparable to those of LINER and Seyfert nuclei. On the other hand, some galaxies, in particular NGC 3627, NGC 4569, and NGC 5866, are very luminous in H_2 but have only modest X-ray–to–H_2 luminosity ratios compared with other H_2 excess galaxies. We assume a power-law spectrum with a standard photon index of −1.8, as adopted by Ho et al. (2001) to extrapolate the total X-ray luminosity to lower photon energies. Under this assumption, the luminosity between 0.2 and 10 keV is only 2 times the luminosity between 2 and 10 keV compiled here. Up to 10% of the intrinsic 1–10 keV luminosity may emerge in the sum of all H_2 transitions (Lepp & McCray 1983), whereas in our comparison we have summed only the three rotational lines *S*(0) to *S*(2). Therefore, pure X-ray excitation of the excess H_2 emission should not be energetically possible even in objects such as NGC 4579 and NGC 5195, which have relatively low H_2–to–X-ray luminosity ratios in Figure 11. Even if the intrinsic emission in soft X-rays were underestimated by a large factor, X-ray excitation would still be unlikely to dominate in most cases. The apparent trend of increasing excess H_2 luminosities with increasing X-ray luminosities in Figure 11 does not imply a direct excitation of H_2 by X-rays, since it could also be understood in the frame of multiphase shocks, produced by supernova remnants or by starburst winds (see below). From near-infrared line ratios, Davies et al. (2005) also reached the conclusion that X-rays do not contribute significantly to the excitation of H_2 in a small sample of AGNs, within regions smaller than those sampled here (about 100 pc).

Supernova remnants are another important source of X-rays. More than half their mechanical energy can be converted to X-rays, mostly with energies below ~500 eV (Draine & Woods 1991), but the X-ray power is converted to H_2 emission in the *S*(0) to *S*(2) lines with low efficiencies, less than 10^{-3} (Draine & Woods 1990). Therefore, in view of the estimates presented in Figure 12 (see the next section for details), heating of H_2 by X-rays from supernova remnants is completely negligible.

7.2. *Heating by Shocks*

For galaxies such as NGC 3627 and NGC 4569, with very high H_2–to–X-ray luminosity ratios, an efficient mechanism has to be invoked to account for the H_2 brightness. It has been shown recently that galactic shocks can convert a very large fraction of the kinetic energy into rotational H_2 emission without producing a lot of X-rays (Appleton et al. 2006). We thus propose that large-scale shocks play a major role. NGC 3627 is an interacting galaxy in the Leo Triplet, characterized by severe morphological and kinematical distortions and, in the center, a massive molecular gas concentration in the form of an asymmetric barlike structure (Zhang et al. 1993), with a peak in the stellar velocity dispersion that is shifted by about 3″ from the nucleus, and probably strong

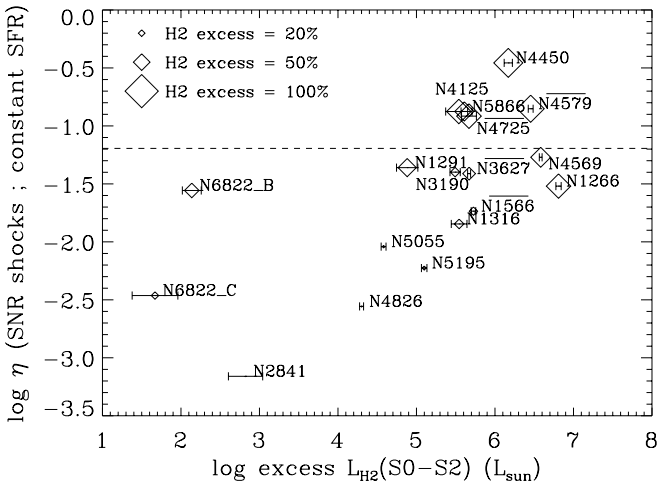

FIG. 12.—Heating efficiency required to account for the excess H_2 emission by supernova remnant shocks [ratio of the power in the sum of the $S(0)$–$S(2)$ lines to the total mechanical power], as a function of the excess H_2 luminosity, defined as in Fig. 11. The dashed line indicates the maximum efficiency expected if all the mechanical power produced by supernova remnants is absorbed in molecular clouds, for the model parameters of Kaufman & Neufeld (1996). The size of the symbols is proportional to the fraction of excess H_2 to total H_2 emission. Seyfert nuclei are marked by an overlying horizontal bar. The regions B and C within NGC 6822 are the only non-AGN targets in this figure.

gas inflow into the nucleus (Afanasiev & Sil'chenko 2005). NGC 4569 is a starburst LINER (Maoz et al. 1998) having recently produced a large number of supernova explosions, triggering the expansion of X-ray, Hα (Tschöke et al. 2001), and synchrotron emission lobes (Chyzy et al. 2006), and also has a circumnuclear ring of molecular gas with strong noncircular motions (Nakanishi et al. 2005). The situation could be similar to NGC 4945, where H_2 emission is seen to follow the innermost part of a starburst outflow, with an extent of $\sim$200 pc (Moorwood et al. 1996). These two examples thus support the idea of a dominant excitation by shocks, triggered by dynamical perturbations and by a starburst wind, respectively.

In order to test the possibility that the excess H_2 emission is caused by supernova remnant shocks, we estimated the required heating efficiencies in the following way. We first computed the star formation rate required to account for the excess H_2 emission, assuming constant star formation, if all the mechanical power is converted to the power emitted by the sum of the $S(0)$ to $S(2)$ lines (using the Starburst99 population synthesis model of Leitherer et al. 1999). We then compared this with the star formation rate estimated from the 24 μm luminosity, using the calibration of Wu et al. (2005) for the same initial mass function. The ratio of the two rates gives an order-of-magnitude estimate of the H_2 heating efficiency η that is needed if supernova shocks are invoked as the dominant heating mechanism, and it is shown in Figure 12 as a function of the excess H_2 luminosity. In this simplified computation, the H_2 excess in the star-forming regions B and C of NGC 6822 can easily be attributed to supernova remnant shocks, as they would imply efficiencies of at most 3%. Besides these regions, supernova remnants are also a sufficient heating source of the excess H_2 for at least six of the LINER and Seyfert nuclei. In NGC 5195, in particular, the necessary heating efficiency (including the fraction of the total mechanical power injected and absorbed in molecular clouds) is very small. Galaxies such as NGC 4450 and NGC 4579, on the other hand, unambiguously require much more power than available in supernova remnants. The excitation source could be shocks triggered by cloud collisions induced by gravitational perturbations, maybe in combination with X-rays.

NGC 1316 (Fornax A) stands out in Figure 7 as having the highest T_1 temperature ($T_1 > 280$ K) and the lowest mass fraction in warm phase (<1%), and the lowest levels up to $J = 4$ are characterized by a single temperature. In this particular case, H_2 may be heated by fast shocks caused by the powerful jet that has produced large-scale radio lobes and that is observed in the form of knots in the inner kiloparsec, which may be a signature of interaction with the interstellar medium, i.e., shocks (Geldzahler & Fomalont 1984). Excitation by FUV radiation and X-rays or by slow shocks would produce a large quantity of H_2 at temperatures between 100 and 300 K (Burton et al. 1992; Maloney et al. 1996), which is ruled out by the data. NGC 1316 is the only galaxy of the sample for which the excess H_2 may be heated by an AGN jet.

Of the 16 H_2 excess galaxies, all have excitation diagrams consistent with $\mathrm{OPR}_{\mathrm{high}\,T} = 3$ (at least in the free-T_1 fits), except NGC 1266, NGC 5866, and NGC 4125. NGC 1266 may be unusual simply by virtue of its significant optical depth, as discussed in § 3.3. This predominance of $\mathrm{OPR}_{\mathrm{high}\,T} = 3$, combined with more elevated temperatures than in H II nuclei on average (Fig. 7), would be consistent with the excess H_2 emission originating in shocks where ortho-para equilibration is fast. It remains, however, difficult to test this idea and to identify the source of these shocks.

8. SUMMARY AND CONCLUSIONS

We present the measurements and results of a survey of the four lowest energy rotational transitions of H_2, $S(0)$ to $S(3)$, in a local sample of 57 galaxies, from the SINGS program. For three galaxies in this sample, higher energy transitions, up to $S(7)$, could be measured. Characterizing the amount and physical conditions of the warm molecular hydrogen phase traced by these lines is of prime interest because molecular hydrogen represents a major mass fraction of the interstellar medium of normal galaxies, and the warm phase itself (gas heated to temperatures of $\approx$100–1000 K) can constitute a substantial fraction of the total H_2.

The emission is measured over areas of median size 0.9 kpc, thus including a large number of distinct star formation sites and molecular clouds. The sample comprises mostly nuclear regions (in 47 massive galaxies and nine dwarf galaxies), of which 45% are optically classified as LINER or Seyfert, as well as 10 extranuclear star formation complexes within a dwarf galaxy and a spiral. With respect to earlier studies of molecular hydrogen emission in galaxies, and particularly rotational lines, which had focused on very bright systems (nearby starbursts and AGNs, as well as ultraluminous galaxies), this paper provides results on the average properties of warm H_2 of relatively faint systems, more representative of the general population of galaxies.

Perhaps the most significant observational results (detailed below) are (1) the tight correlation of the powers emitted by the sum of the $S(0)$ to $S(2)$ lines and by aromatic bands, and the fact that the $F(S0–S2)$/PAH ratio is insensitive to the marked variations in average radiation field intensities existing in our sample; and (2) the existence of nonequilibrium ortho-to-para ratios in the rotational levels, which are weakly correlated with the surface brightness of the H_2 lines. These results call for further modeling in order to be better understood.

Masses and column densities.—The total masses of warm H_2 within our apertures range between 10^5 and close to 3×10^8 $M_\odot$ in galaxy nuclear regions. In star formation complexes of nearby dwarf galaxies (NGC 2915 and NGC 6822), we probe warm H_2 masses down to a few times 10^3 $M_\odot$ within equivalent diameters of 60–250 pc. The mass densities range between 0.2 and 30 $M_\odot$ pc^{-2}. The column densities that we derive are on average of the same order of magnitude as the column densities observed

in individual Galactic PDRs. For systems in which H_2 is predominantly excited by PDRs, assuming that they have similar characteristics to the Orion Bar, this implies that they fill most of the observing beam.

H_2 *mass fraction in the warm phase* ($T \geq 100$ K).—Under a conservative assumption about the distribution of temperatures, we find that the warm H_2 gas makes up between 1% and more than 30% of the total H_2. For star-forming galaxies, the median mass fraction in the warm phase is 10%. The column density nevertheless has a steep inverse dependence on the temperature, and we cannot rule out that the unconstrained cool H_2 component ($70\ \mathrm{K} < T < 100\ \mathrm{K}$) might in some cases dominate the $S(0)$ and $S(1)$ emission and account for most of the H_2 mass.

PDR excitation in star-forming regions.—In H II nuclei, we observe a remarkably narrow range of H_2–to–aromatic band flux ratio. This result argues for PDRs providing most of the power used for H_2 excitation, since aromatic bands are known to arise predominantly from these regions, as defined by Hollenbach & Tielens (1997), which include all the neutral interstellar medium illuminated by FUV photons. Two main excitation mechanisms can be at work simultaneously in PDRs: pumping by FUV photons, followed by fluorescent decay to the ground electronic state, and collisions with hydrogen atoms and molecules heated by photoelectrons or FUV pumping. Comparison with the predictions of PDR models for the ratio of H_2 to FUV luminosity indicates a narrow range of average physical conditions, G_0/n between 0.1 and 1 with the radiation field intensity G_0 in units of 1.6×10^{-3} ergs s^{-1} cm^{-2} and the hydrogen nucleus density n in units of cm^{-3}. The sum of the $S(0)$ to $S(2)$ transitions represents between 2.5×10^{-4} and 7.5×10^{-4} of the total infrared power, and on average 30% of the [Si II] line power. The observed temperatures suggest that the average G_0 varies between about 100 and 5000, and the average n between about 500 and 10^4 cm^{-3}. This seems to imply that H_2 rotational line emission comes mostly from molecular clouds illuminated by OB associations. We have seen, however, that the estimator of these parameters is biased (see § 6.1), and a nonnegligible contribution from less dense regions with less intense radiation fields is not excluded.

Evidence for fluorescence in star-forming regions.—Previous surveys of rotational lines in galaxies had not revealed any departure from thermalization of H_2, which is a consequence of the relatively low critical densities of the lower rotational transitions. By contrast, we find that nearly half the targets in our sample deviate significantly from LTE in having apparent ortho-to-para ratios $\mathrm{OPR}_{\mathrm{high}\ T}$ lower than the equilibrium value of 3. We have seen that this result cannot be an artifact caused by extinction effects. Low values of $\mathrm{OPR}_{\mathrm{high}\ T}$ may thus be interpreted as evidence of fluorescent excitation, which naturally leads to low ortho-to-para ratios in the excited states, occurring in regions of sufficiently low density that ortho-para equilibration by collisions is incomplete. The fraction of relatively diffuse molecular gas in normal galaxies could thus be far from negligible. In order to test this idea, it would be desirable to obtain independent estimates of the average gas density in PDRs. In the absence of any robust estimate of this quantity, we used the surface brightness of the sum of the $S(0)$ to $S(2)$ transitions as a tracer of the coupled variations of n and G_0 to show that the data are compatible with an interpretation of low apparent $\mathrm{OPR}_{\mathrm{high}\ T}$ values in terms of low-density PDRs. In particular, the lowest values occur preferentially in very late-type galaxies, which may have a more diffuse interstellar medium than earlier type galaxies. In the present sample, close to half the star-forming targets have low $\mathrm{OPR}_{\mathrm{high}\ T}$ values. We infer that fluorescence can be the predominant excitation mechanism of rotational H_2 lines in normal star-forming galaxies. In more active galaxies, however, collisional excitation in PDRs is likely to overtake fluorescence, even though the latter still contributes to gas heating. Alternatively, low $\mathrm{OPR}_{\mathrm{high}\ T}$ values may be caused by nonequilibrium PDRs, in which initially cold gas, recently reached by the photodissociation front and heated, has not had enough time to adjust its ortho-to-para ratio. A disadvantage of this scenario is that it does not explain why PDRs would have systematically different properties in targets with $\mathrm{OPR}_{\mathrm{high}\ T} < 3$ and in those with $\mathrm{OPR}_{\mathrm{high}\ T} = 3$. We thus emphasize that the cause of nonequilibrium ortho-to-para ratios in the rotational levels is not well understood at present.

Differences between H II *and LINER/Seyfert nuclei*.—Despite our large observing beam implying that the emission from the immediate vicinity of the nucleus is diluted in the emission from extended areas decoupled from nuclear activity, a large fraction of nuclei classified as LINER or Seyfert distinguish themselves from purely star-forming nuclei in several ways. In a statistical sense, the temperatures of the warm H_2 phase are slightly higher, and as a corollary the mass fractions of warm to total H_2 are lower (with a median of 4% instead of 10% for H II nuclei). The correlation between H_2 and aromatic band emission observed in H II nuclei also breaks down in LINER and Seyfert nuclei. A large number of them have excess emission in the H_2 lines, with respect to aromatic bands and to [Si II], which in general is the brightest cooling line in the mid-infrared range (with possible contributions from both PDRs and H II regions, as well as X-ray–irradiated gas), and, to a lesser degree, with respect to the total infrared emission. The fact that less contrast between the different nuclear categories is seen in the H_2/TIR ratio may partly be due to the fact that estimating the 70 and 160 μm fluxes within our small apertures requires a large extrapolation.

Threshold for nonstellar excitation.—We propose that nuclear ratios $F(S0\text{-}S2)/F_{7.9,\mathrm{dust}} > 10^{-1.94}$, with observables defined as in our study, are indicative of the LINER and Seyfert categories. It should, however, be kept in mind that some sources belonging to these classes are indistinguishable from H II nuclei. This could be thought of as mainly a distance and beam dilution effect, but the H_2/PAH ratio behaves contrary to this expectation, since in the present sample it shows a correlation with distance, rather than an anticorrelation. None of the quantities derived in this paper show any dependence on distance, with this exception of the H_2 excess in LINER and Seyfert nuclei. The fact that it tends to increase with distance could be a selection bias, but it also suggests that the H_2 excess is in general spatially extended. We may also remark that for galaxies like NGC 1377, whose dust emission is interpreted as dominated by an extremely young and opaque starburst (Roussel et al. 2006), the above criterion to select LINER and Seyfert nuclei will not be applicable.

Shock excitation in LINER/Seyfert nuclei.—We interpret the differences in H_2/PAH ratios as a genuine excess of H_2 emission (and not a deficit of the other tracers while preserving H_2), i.e., as requiring at least one additional mechanism to excite H_2 molecules with respect to PDR heating. Excitation by nuclear X-rays seems implausible, as models predict much lower heating efficiencies than what would be necessary to account for the estimated H_2 excess, compared with X-ray luminosities derived from *Chandra* observations. We thus favor excess heating by large-scale shocks, caused either by the collective effect of supernovae in an aging starburst or by dynamical perturbations. An order-of-magnitude estimate suggests that supernova remnant shocks can easily account for the H_2 excess of a fraction of the LINER and Seyfert nuclei (for example, NGC 5195) but do not provide enough mechanical power for the galaxies with the highest H_2/PAH ratios. For the latter, shocks triggered by dynamical perturbations are

the best candidate to supply the excess H_2 heating. In one case, it is conceivable that the excess H_2 emission may be produced by the interaction of a nuclear jet with the interstellar medium, namely, in NGC 1316 (Fornax A). This target has the warmest H_2 of the whole sample, with no evidence for a cool ($T < 300$ K) component, the lowest mass fraction in the warm phase, and is remarkable for its large-scale radio lobes.

Ortho-para thermalization in LINER/Seyfert nuclei.—Consistent with the hypothesis that the additional H_2 may be caused by shocks in which ortho-para equilibration is fast, the excitation diagrams of most galaxies with excess H_2 emission are consistent with ortho-para thermalization ($OPR_{high\ T} = 3$), with three exceptions: NGC 1266 (where we have seen that the apparent $OPR_{high\ T} < 3$ may be a result of high optical depth toward H_2), NGC 5866, and NGC 4125. Note that the latter two galaxies are observed edge-on, so that $OPR_{high\ T} < 3$ could also be an extinction artifact; this would, however, imply that the optical depth derived from the silicate bands is underestimated by large factors (see § 3.3). If excess H_2 emission originated from shocks with $OPR_{high\ T} < 3$ in the latter two galaxies, it would imply that the gas was initially cold and had not had time to reach equilibrium.

The rotational H_2 lines are most often fainter than the forbidden lines in the same wavelength range, in particular [Si II], [Ne II], [Ne III], and [S III] (with no example of an H_2-dominated line spectrum in the present sample), but are among the dominant coolants of molecular gas and provide important constraints on the excitation of the warm molecular interstellar medium, where a large mass fraction of the gas resides in normal galaxies. The results presented here are assumed to be representative of moderate-luminosity galaxies of all types and can serve as a comparison point for future studies of distant galaxies.

Support for this work, part of the *Spitzer Space Telescope* Legacy Science Program, was provided by NASA through an award issued by the Jet Propulsion Laboratory, California Institute of Technology under NASA contract 1407. We thank the referee for a careful review and valued suggestions, and Adam Leroy for a useful discussion.

REFERENCES

Aalto, S., Booth, R. S., Black, J. H., & Johansson, L. E. 1995, A&A, 300, 369
Afanasiev, V. L., & Sil'chenko, O. K. 2005, A&A, 429, 825
Albrecht, M., Chini, R., Krügel, E., Müller, S. A., & Lemke, R. 2004, A&A, 414, 141
Allers, K. N., Jaffe, D. T., Lacy, J. H., Draine, B. T., & Richter, M. J. 2005, ApJ, 630, 368
Appleton, P. N., et al. 2006, ApJ, 639, L51
Bajaja, E., Krause, M., Wielebinski, R., & Dettmar, R. J. 1991, A&A, 241, 411
Bally, J., & Lane, A. P. 1982, ApJ, 257, 612
Beck, S. C., Lacy, J. H., & Geballe, T. R. 1979, ApJ, 234, L213
Beckwith, S., Gatley, I., & Persson, S. E. 1978, ApJ, 219, L33
Black, J. H., & Dalgarno, A. 1976, ApJ, 203, 132
Böker, T., Lisenfeld, U., & Schinnerer, E. 2003, A&A, 406, 87
Boulanger, F., Falgarone, E., Puget, J. L., & Helou, G. 1990, ApJ, 364, 136
Braine, J., Combes, F., Casoli, F., Dupraz, C., Gerin, M., Klein, U., Wielebinski, R., & Brouillet, N. 1993, A&AS, 97, 887
Brooks, K. J., Burton, M. G., Rathborne, J. M., Ashley, M. C., & Storey, J. W. 2000, MNRAS, 319, 95
Burton, M. G., Brand, P. W., Geballe, T. R., & Webster, A. S. 1989, MNRAS, 236, 409
Burton, M. G., Hollenbach, D. J., & Tielens, A. G. 1992, ApJ, 399, 563
Chandar, R., Bianchi, L., & Ford, H. C. 2000, AJ, 120, 3088
Chyzy, K. T., Soida, M., Bomans, D. J., Vollmer, B., Balkowski, Ch., Beck, R., & Urbanik, M. 2006, A&A, 447, 465
Claussen, M. J., & Sahai, R. 1992, AJ, 103, 1134
Contini, T., Wozniak, H., Considere, S., & Davoust, E. 1997, A&A, 324, 41
Curran, S. J., Polatidis, A. G., Aalto, S., & Booth, R. S. 2001, A&A, 368, 824
Dale, D. A., & Helou, G. 2002, ApJ, 576, 159
Dale, D. A., et al. 2006, ApJ, 646, 161
———. 2007, ApJ, 655, 863
Dame, T. M., Hartmann, D., & Thaddeus, P. 2001, ApJ, 547, 792
Davies, R. I., Sternberg, A., Lehnert, M., & Tacconi-Garman, L. E. 2003, ApJ, 597, 907
Davies, R. I., Sternberg, A., Lehnert, M. D., & Tacconi-Garman, L. E. 2005, ApJ, 633, 105
Désert, F. X., & Dennefeld, M. 1988, A&A, 206, 227
Draine, B. T., & Li, A. 2007, ApJ, 657, 810
Draine, B. T., Roberge, W. G., & Dalgarno, A. 1983, ApJ, 264, 485
Draine, B. T., & Woods, D. T. 1990, ApJ, 363, 464
———. 1991, ApJ, 383, 621
Draine, B. T., et al. 2007, ApJ, 663, 866
Elfhag, T., Booth, R. S., Hoeglund, B., Johansson, L. E., & Sandqvist, A. 1996, A&AS, 115, 439
Falgarone, E., Verstraete, L., Pineau des Forêts, G., & Hily-Blant, P. 2005, A&A, 433, 997
Fazio, G., et al. 2004, ApJS, 154, 10
Fuente, A., Martin-Pintado, J., Rodriguez-Fernandez, N. J., Rodriguez-Franco, A., de Vicente, P., & Kunze, D. 1999, ApJ, 518, L45
Gatley, I., Beattie, D. H., Lee, T. J., Jones, T. J., & Hyland, A. R. 1984, MNRAS, 210, 565
Gatley, I., et al. 1987, ApJ, 318, L73
Gautier, T. N., Fink, U., Treffers, R. R., & Larson, H. P. 1976, ApJ, 207, L129
Geldzahler, B. J., & Fomalont, E. B. 1984, AJ, 89, 1650
Giard, M., Bernard, J. P., Lacombe, F., Normand, P., & Rouan, D. 1994, A&A, 291, 239
Gordon, M. A. 1991, ApJ, 371, 563
Graham, J. R., Serabyn, E., Herbst, T. M., Matthews, K., Neugebauer, G., Soifer, B. T., Wilson, T. D., & Beckwith, S. 1993, AJ, 105, 250
Habart, E., Boulanger, F., Verstraete, L., Pineau des Forêts, G., Falgarone, E., & Abergel, A. 2003, A&A, 397, 623
Helfer, T. T., & Blitz, L. 1993, ApJ, 419, 86
Helfer, T. T., Thornley, M. D., Regan, M. W., Wong, T., Sheth, K., Vogel, S. N., Blitz, L., & Bock, D. C.-J. 2003, ApJS, 145, 259
Helou, G. 1986, ApJ, 311, L33
Helou, G., Khan, I. R., Malek, L., & Boehmer, L. 1988, ApJS, 68, 151
Helou, G., Malhotra, S., Hollenbach, D. J., Dale, D. A., & Contursi, A. 2001, ApJ, 548, L73
Helou, G., et al. 2004, ApJS, 154, 253
Herbst, T. M., Beckwith, S. V., Glindemann, A., Tacconi-Garman, L. E., Kroker, H., & Krabbe, A. 1996, AJ, 111, 2403
Herbst, T. M., Graham., J. R., Tsutsui, K., Beckwith, S., Matthews, K., & Soifer, B. T. 1990, AJ, 99, 1773
Higdon, S. J., Armus, L., Higdon, J. L., Soifer, B. T., & Spoon, H. W. 2006, ApJ, 648, 323
Ho, L. C., Filippenko, A. V., & Sargent, W. L. 1997, ApJS, 112, 315
Ho, L. C., et al. 2001, ApJ, 549, L51
Hollenbach, D. J., & Tielens, A. G. 1997, ARA&A, 35, 179
Horellou, C., Black, J. H., van Gorkom, J. H., Combes, F., van der Hulst, J. M., & Charmandaris, V. 2001, A&A, 376, 837
Houck, J. R., et al. 2004, ApJS, 154, 18
Hubble, E. 1925, ApJ, 62, 409
Huber, K. P., & Herzberg, G. 1979, Constants of Diatomic Molecules (New York: Van Nostrand)
Israel, F. P. 2005, A&A, 438, 855
Israel, F. P., & Baas, F. 1999, A&A, 351, 10
Israel, F. P., Baas, F., Rudy, R. J., Skillman, E. D., & Woodward, C. E. 2003, A&A, 397, 87
Israel, F. P., Tacconi, L. J., & Baas, F. 1995, A&A, 295, 599
Johnson, K. E., Indebetouw, R., & Pisano, D. J. 2003, AJ, 126, 101
Kaufman, M. J., & Neufeld, D. A. 1996, ApJ, 456, 611
Kaufman, M. J., Wolfire, M. G., & Hollenbach, D. J. 2006, ApJ, 644, 283
Kenney, J. D., & Young, J. S. 1988, ApJS, 66, 261
Kennicutt, R. C., Jr., et al. 2003, PASP, 115, 928
———. 2007, ApJ, in press
Kilgard, R. E., et al. 2005, ApJS, 159, 214
Kim, D. W., & Fabbiano, G. 2003, ApJ, 586, 826
Kinman, T. D., Green, J. R., & Mahaffey, C. T. 1979, PASP, 91, 749
Knapen, J. H., Beckman, J. E., Cepa, J., & Nakai, N. 1996, A&A, 308, 27
Knop, R. A., Armus, L., Matthews, K., Murphy, T. W., & Soifer, B. T. 2001, AJ, 122, 764
Kohno, K., Ishizuki, S., Matsushita, S., Vila-Vilaró, B., & Kawabe, R. 2003, PASJ, 55, L1

Kohno, K., Tosaki, T., Matsushita, S., Vila-Vilaó, B., Shibatsuka, T., & Kawabe, R. 2002, PASJ, 54, 541
Larkin, J. E., Armus, L., Knop, R. A., Soifer, B. T., & Matthews, K. 1998, ApJS, 114, 59
Lee, H., Skillman, E. D., Cannon, J. M., Jackson, D. C., Gehrz, R. D., Polomski, E. F., & Woodward, C. E. 2006, ApJ, 647, 970
Leitherer, C., et al. 1999, ApJS, 123, 3
Leon, S., Combes, F., & Menon, T. K. 1998, A&A, 330, 37
Lepp, S., & Dalgarno, A. 1996, A&A, 306, L21
Lepp, S., & McCray, R. 1983, ApJ, 269, 560
Leroy, A., Bolatto, A. D., Simon, J. D., & Blitz, L. 2005, ApJ, 625, 763
Li, A., & Draine, B. T. 2001, ApJ, 554, 778
Low, F. J., et al. 1984, ApJ, 278, L19
Lutz, D., Sturm, E., Genzel, R., Moorwood, A. F. M., Alexander, T., Netzer, H., & Sternberg, A. 2000, ApJ, 536, 697
Malhotra, S., et al. 2001, ApJ, 561, 766
Maloney, P., & Black, J. H. 1988, ApJ, 325, 389
Maloney, P. R., Hollenbach, D. J., & Tielens, A. G. 1996, ApJ, 466, 561
Mandy, M. E., & Martin, P. G. 1993, ApJS, 86, 199
Maoz, D., Koratkar, A., Shields, J. C., Ho, L. C., Filippenko, A. V., & Sternberg, A. 1998, AJ, 116, 55
Mauersberger, R., Henkel, C., Walsh, W., & Schulz, A. 1999, A&A, 341, 256
Meijerink, R., & Spaans, M. 2005, A&A, 436, 397
Moneti, A., Stolovy, S., Blommaert, J. A., Figer, D. F., & Najarro, F. 2001, A&A, 366, 106
Moorwood, A. F., & Oliva, E. 1988, A&A, 203, 278
Moorwood, A. F., van der Werf, P. P., Kotilainen, J. K., Marconi, A., & Oliva, E. 1996, A&A, 308, L1
Mouri, H., Kawara, K., Taniguchi, Y., & Nishida, M. 1990, ApJ, 356, L39
Nakanishi, H., Sofue, Y., & Koda, J. 2005, PASJ, 57, 905
Nemmen, R. S., Storchi-Bergmann, T., Yuan, F., Eracleous, M., Terashima, Y., & Wilson, A. S. 2006, ApJ, 643, 652
Neufeld, D. A., & Kaufman, M. J. 1993, ApJ, 418, 263
Nishiyama, K., & Nakai, N. 2001, PASJ, 53, 713
Pagel, B. E., Edmunds, M. G., & Smith, G. 1980, MNRAS, 193, 219
Parmar, P. S., Lacy, J. H., & Achtermann, J. M. 1991, ApJ, 372, L25
Planesas, P., Colina, L., & Perez-Olea, D. 1997, A&A, 325, 81
Polk, K. S., Knapp, G. R., Stark, A. A., & Wilson, R. W. 1988, ApJ, 332, 432
Puxley, P. J., Hawarden, T. G., & Mountain, C. M. 1988, MNRAS, 234, 29P
Quillen, A. C., Alonso-Herrero, A., Rieke, M. J., Rieke, G. H., Ruiz, M., & Kulkarni, V. 1999, ApJ, 527, 696
Reach, W. T., Rho, J., Jarrett, T. H., & Lagage, P. O. 2002, ApJ, 564, 302
Rieke, G., et al. 2004, ApJS, 154, 25
Rigopoulou, D., Kunze, D., Lutz, D., Genzel, R., & Moorwood, A. F. 2002, A&A, 389, 374
Rotaciuc, V., Krabbe, A., Cameron, M., Drapatz, S., Genzel, R., Sternberg, A., & Storey, J. W. V. 1991, ApJ, 370, L23
Roussel, H., et al. 2006, ApJ, 646, 841
Sage, L. J. 1989, ApJ, 344, 200
———. 1993, A&A, 272, 123
Sage, L. J., Salzer, J. J., Loose, H. H., & Henkel, C. 1992, A&A, 265, 19
Sakamoto, K., Okumura, S. K., Ishizuki, S., & Scoville, N. Z. 1999, ApJS, 124, 403
Satyapal, S., Dudik, R. P., O'Halloran, B., & Gliozzi, M. 2005, ApJ, 633, 86
Satyapal, S., Sambruna, R. M., & Dudik, R. P. 2004, A&A, 414, 825
Sellgren, K., Tokunaga, A. T., & Nakada, Y. 1990, ApJ, 349, 120
Sheth, K., Vogel, S. N., Regan, M. W., Thornley, M. D., & Teuben, P. J. 2005, ApJ, 632, 217
Shioya, Y., Tosaki, T., Ohyama, Y., Murayama, T., Yamada, T., Ishizuki, S., & Taniguchi, Y. 1998, PASJ, 50, 317
Shull, J. M., & Beckwith, S. 1982, ARA&A, 20, 163
Shull, J. M., & Hollenbach, D. J. 1978, ApJ, 220, 525
Smith, J. D., et al. 2004, ApJS, 154, 199
———. 2007a, ApJ, 656, 770
———. 2007b, PASP, in press (arXiv: 0708.3745)
Sofue, Y., Koda, J., Nakanishi, H., Onodera, S., Kohno, K., Tomita, A., & Okumura, S. K. 2003, PASJ, 55, 17
Sternberg, A., & Dalgarno, A. 1989, ApJ, 338, 197
Sternberg, A., & Neufeld, D. A. 1999, ApJ, 516, 371
Strong, A. W., et al. 1988, A&A, 207, 1
Sugai, H., Malkan, M. A., Ward, M. J., Davies, R. I., & McLean, I. S. 1997, ApJ, 481, 186
Tacconi, L. J., Tacconi-Garman, L. E., Thornley, M., & van Woerden, H. 1991, A&A, 252, 541
Tanaka, M., Hasegawa, T., Hayashi, S. S., Brand, P. W., & Gatley, I. 1989, ApJ, 336, 207
Taniguchi, Y., Murayama, T., Nakai, N., Suzuki, M., & Kameya, O. 1994, AJ, 108, 468
Terebey, S., & Fich, M. 1986, ApJ, 309, L73
Thompson, R. I., Lebofsky, M. J., & Rieke, G. H. 1978, ApJ, 222, L49
Tielens, A. G., & Hollenbach, D. 1985, ApJ, 291, 722
Tielens, A. G., Meixner, M. M., van der Werf, P. P., Bregman, J., Tauber, J. A., Stutzki, J., & Rank, D. 1993, Science, 262, 86
Timmermann, R. 1998, ApJ, 498, 246
Treffers, R. R. 1979, ApJ, 233, L17
Treffers, R. R., Fink, U., Larson, H. P., & Gautier, T. N. 1976, ApJ, 209, 793
Tschöke, D., Bomans, D. J., Hensler, G., & Junkes, N. 2001, A&A, 380, 40
Usero, A., García-Burillo, S., Fuente, A., Martín-Pintado, J., & Rodríguez-Fernández, N. J. 2004, A&A, 419, 897
Valentijn, E. A., van der Werf, P. P., de Graauw, T., & de Jong, T. 1996, A&A, 315, L145
Vila-Vilaró, B., Taniguchi, Y., & Nakai, N. 1998, AJ, 116, 1553
Voit, G. M. 1992, MNRAS, 258, 841
Welch, G. A., & Sage, L. J. 2003, ApJ, 584, 260
Wiklind, T., Combes, F., & Henkel, C. 1995, A&A, 297, 643
Wilgenbus, D., Cabrit, S., Pineau des Forêts, G., & Flower, D. R. 2000, A&A, 356, 1010
Wu, H., Cao, C., Hao, C. N., Liu, F.-S., Wang, J.-L., Xia, X.-Y., Deng, Z.-G., & Young, C. K.-S. 2005, ApJ, 632, L79
Yao, L., Seaquist, E. R., Kuno, N., & Dunne, L. 2003, ApJ, 588, 771
Young, J. S., et al. 1995, ApJS, 98, 219
Zhang, X., Wright, M., & Alexander, P. 1993, ApJ, 418, 100